Whole Genome and Embryo Transcriptome Analysis of Vertebrate Identifies *nxhl* Controlling Angiogenesis by Targeting VE-PTP

Honglin Luo[1, 2*], Yongde Zhang[1, *], Changmian Ji [3*], Yongzhen Zhao[1 *], Jinxia Peng [1*], Xiuli Chen[1], Yin Huang[1], Qingyun Liu[1], Pingping He[1], Pengfei Feng[1], Chunling Yang[1], Pinyuan Wei[1], Haiyan Yu[3], Hongkun Zheng[3, #], Yong Lin[1, #], Xiaohan Chen[1, #]

[1]Guangxi Key Laboratory for Aquatic Genetic Breeding and Healthy Aquaculture, Guangxi Academy of Fishery Sciences, Nanning, 530021, China

[2] Affiliated Tumor Hospital of Guangxi Medical University, Nanning, 530021, China

[3] Biomarker Technologies, Beijing, 101300, China.

[*] These authors contributed equally to this work.

[#]Prime correspondence to: Xiaohan Chen. Hongkun zheng and YongLin are also corresponding authors

Running title: *Nxhl* controls angiogenesis by targeting VE-PTP

Subject Terms:

Animal Models of Human Disease

Basic Science Research

Developmental Biology

Gene Expression and Regulation

Cardiovascular Disease

Address Correspondence to:

Mr. Xiaohan Chen (xhchensci@126.com) and Mr. Yonglin (linnn2005@126.com) : NO. 8, Qingshan Road, Guangxi Key Laboratory for Aquatic Genetic Breeding and Healthy Aquaculture, Guangxi Institute of Fishery Sciences, Nanning, 530021, China.

Mr. Hongkun zheng (zhenghk@biomarker.com.cn): Biomarker Technologies, Beijing, 101300, China.

ABSTRACT

BACKGROUND: Angiogenesis is closely associated with angiogenesis-dependent diseases including cancers and ocular diseases. Anti-angiogenic therapeutics have been focusing on the (VEGF)/VEGFR signaling axis. However, the clinical resistance, high cost and frequent administration of anti-VEGF drugs make it urgent to discover novel angiogenic pathways.VE-PTP (*ptprb*) is a novel target with great anti-angiogenic potential. However, it is unclear whether upstream signaling pathways targeting VE-PTP exist in angiogenesis.

METHODS: Whole genome and embryo transcriptome sequencing were applied to discover the new gene *nxhl*. Transgenic zebrafish model, morpholino knockdown and small interfering RNA were used to explore the role of *nxhl* in angiogenesis both *in vitro* and *in vivo.* RNA pulldown, RIP and ChIRP-MS were used to identify interactions between RNA and protein.

RESULTS: We discovered a novel zebrafish gene *nxhl* which is a homologue of the conserved gene *nxh* that co-expressed with some key genes essential for embryo development in vertebrate. *Nxhl* deletion causes angiogenesis defects in embryo. Moreover, *nxhl* is essential to mediate effects of angiogenesis *in vivo* and *in vitro*, and *ptprb* depletion duplicates the phenotypes of *nxhl* deficiency. Importantly, *nxhl* acts upstream of *ptprb* and regulates many extreme important *ptprb*-linked angiogenic genes by targeting VE-PTP (*ptprb*) through interactions with NCL. Notably, *nxhl* deletion decreases the phosphorylation of NCL T76 and increases the acetylation of NCL K88, suggesting *nxhl* may regulate downstream VE-PTP signaling pathways by mediation of NCL posttranslational modification. This is the first description of the interaction between *nxhl* and NCL, NCL and VE-PTP (*ptprb*), uncovering a novel *nxhl*-NCL-VE-PTP signaling pathway on angiogenesis regulation.

CONCLUSIONS: Our study identifies *nxhl* controlling angiogenesis by targeting VE-PTP through interactions with NCL, uncovering novel upstream controllers of VE-PTP. This *nxhl*-NCL-VE-PTP pathway may be a therapeutic target in the treatment of angiogenesis-dependent diseases.

Key Words: Angiogenesis, *nxhl*, VE-PTP, *ptprb,* nucleolin, WGD, cancer.

Clinical Perspective

What Is New?

- We report a novel *nxhl*-NCL-VE-PTP signaling pathway that controls angiogenesis.
- We for the first time demonstrate that *nxhl* interacts with NCL which simultaneously binds to VE-PTP that plays key roles on EC adherens junction, integrity and vascular homeostasis.
- *Nxhl* also controls some other crucial VE-PTP-linked downstream angiogenic genes (such as Tie2, VEGFaa, VEGFR2, Erbb2, S1pr1 and Hey2) which explain the phenotypes induced by the *nxhl* deficiency.
- Our study indicates the key role of *nxhl* on controlling angiogenesis as an upstream regulator of VE-PTP.

What Are the Clinical Implications?

- There are several ongoing researches investigating the utility of VE-PTP or NCL inhibitors on treatment of angiogenesis-dependent diseases including a range of cancers and nonneoplastic diseases, such as AMD, DME, RA and atherosclerosis.
- Targeting the *nxhl*-NCL-VE-PTP pathway may facilitate therapeutic angiogenesis in patients with cancers or ocular diseases such as DME.
- Our study highlights the great potential of *nxhl* on anti-angiogenic therapeutics by targeting VE-PTP.

Angiogenesis is a process of new blood-vessel spreading that is orchestrated by various angiogenic factors. It plays critical roles in reproduction, organ development and wound repair. Pathologically, it is closely related to "angiogenesis-dependent diseases" including a range of tumors and nonneoplastic diseases, such as age-related macular degeneration (AMD) ,[1] diabetic macular edema (DME) ,[2] rheumatoid arthritis (RA)[3] and atherosclerosis.[4] Judah Folkman suggested to consider angiogenesis as an 'organizing principle' in biology.[5] This conception shifted therapeutic strategies from tumor cell-centered to anti-angiogenesis-centered.[6] In the past decades, milestone discoveries of anti-angiogenic therapeutics have been mainly focused on the vascular endothelial growth factor (VEGF)/VEGFR signaling axis. Various inhibitors of this axis, such as Ramucirumab, have been approved for several solid cancers by FDA.[7] Over 3000 anti-angiogenic drugs have been registered clinical trials for cancer treatment and ocular neovascular diseases,[8] highlighting the significant value of anti-angiogenic drugs for clinical applications. However, in the clinical setting, simply blocking the existing VEGF signaling pathway or other angiogenic pathways appears to be less effective for advanced cases and often causes treatment resistance.[9] High cost of currently used anti-VEGF drugs and their frequent dosing make new drugs targeting novel angiogenic pathways clinically necessary and highly desirable.

We specially concern the protein vascular endothelial protein tyrosine phosphatase (VE-PTP, namely *ptprb* in zebrafish) in endothelial cells (ECs), which determine the permeability and integrity of the blood vessel wall and thereby is essential for angiogenesis. VE-PTP is a member of the R3-subclass of R-PTPs and consists of 2251 amino acids with 18 domains.[10] It is indispensable during mouse vessel development[11-13] due to the overactivated Tie2 and increased vessel enlargement.[11, 12, 14] Evidence shows that VE-PTP plays crucial roles in angiogenesis, EC adherens junction, integrity and vascular homeostasis.[12, 15-18] It binds to VEGFR2, resulting in increase of VEGFR2 phosphorylation and activation.[19] It also binds to Tie2 and negatively controls Tie2-induced vascular remodeling and angiogenesis by dephosphorylation.[14]

Suppressing VE-PTP, either by genetic deletion or specific VE-PTP inhibitor (AKB-9778 or ARP-1536) activates Tie2 and thereby regulates EC permeability, integrity and angiogenesis.[20, 21] Its specific inhibitor AKB-9778 has been investigated in cancer[22, 23] and retinal neovascularization,[24, 25] such as breast cancer[26] and DME,[28] and has exhibited its great clinical potential. Logically, targeting the upstream genes that directly or indirectly interact with VE-PTP might be a promising strategy to overcome limitations of current anti-VEGF agents. However, few *in vivo* studies have been conducted to investigate how VE-PTP is regulated by its upstream regulators. Notably, such regulators are still unreported.

Nucleolin (NCL) is also a highly conserved gene that highly expressed in ECs. [26, 27] Cell surface NCL plays crucial roles in the regulation of angiogenesis and tumorigenesis via interactions with various ligands, such as VEGF,[26] EGFR,[28] endostatin,[29] and HER2 (ErbB2).[30] For instance, VEGF is required for NCL cell surface localization in ECs, which strengthens its contribution to the angiogenesis.[31, 32] In addition, inhibition of cell surface NCL in ECs significantly suppresses the EC migration and prevents capillary tubule formation.[31] Previous researches demonstrate that anti-NCL pseudopeptides N6L impairs angiogenesis both *in vitro* and *in vivo* by targeting ECs and tumor vessels.[33, 34] Increased NCL expression is related to worse prognosis of many cancers, such as diffuse large B-cell lymphoma[35] and pancreatic ductal cancer. [34] For now, a variety of aptamers or antibodies targeting NCL, such as AS1411, are under clinical investigation for anticancer treatment and demonstrating promising perspectives,[36] highlighting its potential as a therapeutic target for anti-cancer therapy.

Similar functions of VE-PTP and NCL on angiogenesis provide us clues for further study. So far, it is unclear whether both genes closely associate and thereby mediate angiogenesis process. This should be investigated in an advanced model that facilitates *in vivo* angiogenesis assay. Zebrafish is such a valuable model system for investigation of vascular development. Experimental evidences have indicated that developmental angiogenesis in the zebrafish embryo might be an useful tool for angiogenesis research in

vertebrate because of its high similarity vascular network formation and expression patterns of key genes with humans and other vertebrates. [37, 38] The transparency and external development of embryo and the ability to produce various transgenic germ line fish, as well as the small size and rapid development make vasculature manipulation in zebrafish feasible and more cost-effective.[39] Conserved angiogenic signaling pathways make zebrafish as an ideal system for human angiogenesis researches and anti-angiogenic or anti-cancer drug screening.[40, 41]

Herein, we identified a novel conserved gene *nxhl*, a homologue of *nxh* which is reserved after whole genome duplication (WGD) in a teleost embryo transcriptome, by combination genome and embryo transcriptome and zebrafish model. *Nxhl* strongly controls angiogenesis both *in vitro* and *in vivo*, and acts as a critical upstream regulator of VE-PTP through interactions with NCL that binds to VE-PTP. It is a potential therapeutic target for angiogenesis-dependent diseases.

METHODS

Materials and raw data that support the findings of this study are available upon request to the corresponding authors. A detailed description of genome sequencing associated Materials and Methods is available in the Supplemental information.

Zebrafish Care and Maintenance

Adult wild-type AB strain zebrafish were maintained at 28.5°C on a 14 h light/10 h dark cycle. [42] Five to six pairs of zebrafish were set up for nature mating every time. On average, 200–300 embryos were generated. Embryos were maintained at 28.5°C in fish water (0.2% Instant Ocean Salt in deionized water). The embryos were washed and staged according to.[43] The establishment and characterization of the *TG (zlyz:EGFP)* transgenic lines have been described elsewhere.[39, 44] The zebrafish facility at SMOC (Shanghai Model

147 Organisms Center, Inc.) is accredited by the Association for Assessment and Accreditation of Laboratory
148 Animal Care (AAALAC) International.
149
150 **Zebrafish Microinjections**
151 Gene Tools, LLC (http://www.gene-tools.com/) designed the morpholino (MO). Antisense MO (GeneTools)
152 were microinjected into fertilized one-cell stage embryos according to standard protocols.[39] Translation-
153 blocking (ATG-MO) and splice-blocking morpholinos of the *nxhl* (zgc:113227, NM_001014319.2) and
154 *ptprb* (NM_001316727.1) were designed, respectively. The standard control morpholino was used as Control
155 MO (Gene Tools). The amount of the MOs used for injection was as follows: Control MO, ATG-MO and
156 splice-blocking -MO, 4 ng per embryo. Effectiveness of *nxhl* and *ptprb* knockdown was confirmed by qPCR
157 (Quantitative Real-Time PCR). For the morpholinos and primers, see Table S28.
158
159 **Zebrafish Angiogenesis Studies and Image Acquisition**
160 To evaluate blood vessel formation in zebrafish, fertilized one-cell *fli1a-EGFP* transgenic lines embryos
161 were injected with 4 ng *nxhl*-e1i1-MO, *nxhl*-ATG-MO, control-MO, and *ptprb*-e4i4-MO, *ptprb*-ATG-MO,
162 control-MO, respectively. At 52 phf (*nxhl* MO) and 2 dpf (*ptprb* MO), embryos were dechorionated,
163 anesthetized with 0.016% MS-222 (tricaine methanesulfonate, Sigma-Aldrich, St. Louis, MO). Zebrafish
164 were then oriented on the lateral side (anterior, left; posterior, right; dorsal, top), and mounted with 3%
165 methylcellulose in a depression slide for observation by fluorescence microscopy. The phenotypes of
166 complete intersegmental vessels (ISVs) (i.e., the number of ISVs that connect the DA to the DLAV),
167 parachordal vessels (PAV) and caudal vein plexus (CVP) were analyzed. Embryos and larvae were
168 analyzed with Nikon SMZ 1500 Fluorescence microscope and subsequently photographed with digital
169 cameras. A subset of images was adjusted for levels, brightness, contrast, hue and saturation with Adobe

Photoshop 7.0 software (Adobe, San Jose, California) to visualize the expression patterns optimally. Quantitative image analyses processed using image based morphometric analysis (NIS-Elements D3.1, Japan) and ImageJ software (U.S. National Institutes of Health, Bethesda, MD, USA; http://rsbweb.nih.gov/ij/). Inverted fluorescent images were used for processing. Positive signals were defined by particle number using ImageJ. Ten animals for each treatment were quantified and the total signal per animal was averaged.

Quantitative Real-Time PCR

Total RNA was extracted from 30 to 50 embryos per group in Trizol (Roche) according to the manufacturer's instructions. RNA was reverse transcribed using the PrimeScript RT reagent Kit with gDNA Eraser (Takara). Quantification of gene expression was performed in triplicates using Bio-rad iQ SYBR Green Supermix (Bio-rad) with detection on the Realplex system (Eppendorf). Relative gene expression quantification was based on the comparative threshold cycle method ($2^{-\Delta\Delta Ct}$) using *ef1α* as an endogenous control gene. qPCR on HUVECs were performed as similar procedures. All of the primers are listed in Table S28.

RNA-Seq

Control MO-injected embryos and embryos injected with *nxhl* MO at 3 dpf were frozen for RNA-seq analysis. Three biological replicates of 30 embryos each were analyzed in each group. RNA was purified using RNAqueous Total RNA isolation kit (Thermo Fisher). Libraries were prepared with TruSeq RNA library Prep kit v2 (Illumina) according to the manufacturer's protocol. Libraries were sequenced at the CCHMC Core Facility using Illumina HiSeq 2500 device (Illumina) to generate 75 bp paired-end reads. Quality of the RNA-Seq reads was checked using Fastqc [http://www.bioinformatics.bab raham.ac.uk/projects/fastqc/]. All of the low-quality reads were trimmed using trimmomatic [http://www.usadellab.org/cms/?page=trimmo

matic]. The trimmed RNA-Seq reads were mapped and quantified to latest Zebrafish genome assembly GRCz10 for each sample at default thresholds using RSEM [http://deweylab.github.io/RSEM/]. The mRNA levels were identified using TopHat v2.0.9 and Cufflinks and normalized by the Fragments Per Kilobase of exon model per Million mapped reads (FPKM). Differential expression was analyzed by using CSBB's [https://github.com/skygenomics/CSBB-v1.0]. Criteria of false discovery rate (FDR) <0.01 and fold changes <0.5 or >2.0 (<−1 or >1 log2 ratio value, p value < 0.05) were used to identify differentially expressed genes. Gene Ontology (GO) annotation, domain annotation, Kyoto Encyclopedia of Genes and Genomes (KEGG) pathway annotation and enrichment were performed using ToppGene [https://top gene.cchmc.org/].

Transwell Migration and Invasion Assays

To examine the function of human Harbi1, the homologous gene of *nxh* and *nxhl*, siRNA targeting human Harbi1 gene (NM_173811.4) was designed (see Table S28). HUVECs cells (ATCC, Manassas, Virginia, USA) were cultured in DMEM/F12 (Hyclone, USA) with 10% FBS (Gibco BRL. Co. Ltd.) and 1% penicillin-streptomycin (Sangon Biotech, China.) at 37°C in 5% CO_2 incubator. Three experimental groups HUVECs, HUVECs + si-Harbi1 NC and HUVECs+si-Harbi1 were set and 30 pmol si-Harbi1 per well in the 24-well plates (Corning-Costa) were transferred using 9 μl Lipofectamine RNAi MAX Reagent (Invitrogen, USA). The cell migration and invasion capacity of Harbi1 on HUVECs cells were determined by transwell insert chambers (Corning, NY, USA) covered with or without 50 μl of Matrigel (1:3 dilution, BD, NJ, USA). Cells were then harvested and dissociated into a single-cell suspension. 5×10^4 cells in serum-free medium were added to the upper chamber and 600 μl of 20% FBS-containing medium was added to the lower chamber. The chambers were then incubated for 72 h (5% CO_2, 37 °C). Cells on the upper chamber were discarded, while cells on the lower chamber were fixed with 4% paraformaldehyde for 30 min and then stained with 0.1% crystal violet for 10 min. Cells that underwent migration or invasion were counted in triplicates in microscopic fields. The migration of nucleolin (NM_005381.3) was also examined by similar

217 protocol above. The siRNA of NCL is listed in Tale S28.

218

219 **Tube Formation Assay**

220 The HUVECs' culture conditions and experimental set were identical to the transwell migration and invasion
221 assays. Thirty pmol si-Harbi1 or si-NCL per well of the 24-well plates (Corning-Costa) were transferred by
222 using 9 μl Lipofectamine RNAi MAX Reagent (Invitrogen, USA). Matrigel (250 μl per well, BD
223 Biosciences, USA) was added to the plates and cultured at 37 °C for 30 min. Then, a suspension containing
224 5×10^4 HUVECs was added to each well and cultured at 37℃ in 5% CO_2 incubator. A final concentration of
225 50 μM Calcein-AM (Solarbio, China) per well was added to the plates and incubated for 30 min at 37℃. Six
226 hours later, the tube formation was observed and counted under the fluorescence microscope. The number
227 of formed tubes represented the tube forming capability of HUVECs.

228

229 **Comprehensive Identification of RNA-binding Proteins by Mass Spectrometry (ChIRP-MS)**

230 Zebrafish embryos (3 dpf) were collected and a total of 2×10^7 cells were prepared and re-suspended in
231 precooled PBS buffer followed by crosslinking with 3% formaldehyde for 30 min at 25℃. The reaction was
232 stopped by incubation with 0.125 M glycine for 5 min. After centrifugation at 1,000 RCF for 3 min, the pre-
233 binding probes (100 pmol per 2×10^7 cells; probes see Table S28) were incubated with streptavidin beads
234 for 30 min. The unbound probes were removed by washing three times. The beads with probes were
235 incubated with the cell lysate and hybridized at 37℃ overnight with shaking. All of the beads were washed
236 3 times with pre-warmed wash buffer for 5 min. A small aliquot (1/20 of the beads) of post-ChIRP beads
237 were reserved for RNA extraction and qPCR analysis. Then 100 μL of elution buffer (12.5mM biotin, 7.5mM
238 HEPES pH 7.5, 75mM NaCl, 1.5mM EDTA, 0.15% SDS, 0.075% sarkosyl, 0.02% Na-Deoxycholate, and

20 U benzonase) was added and the protein was eluted at 37°C for 1 h. The eluent was transferred to a fresh low-binding tube and the beads were eluted again with 100 μL of elution buffer. The two eluents were combined and the reverse-crosslinking was performed at 95°C for 30 min. The protein was precipitated with 0.1% SDC and 10% TCA by centrifugation at 4°C for 2 h. The pellets were then washed with precooled 80% acetone three times before the proteins were used for mass spectrometry (MS) analysis. Then 5 μL peptides of each sample were collected and separated by nano-UPLC easy-nLC1200 liquid phase system before they were detected using an on-line mass spectrometer (Q-Exactive) at a solution of 70,000. All of the original MS data were queried against zebrafish protein database (UNIPROT_zebrafish_2016_09). Only those proteins with an FDR < 0.01 and an adjusted *p*-value < 0.05 were considered differentially expressed. The identified proteins were then further examined using bioinformatics, including GO) and KEGG pathway annotations.

Nxhl Protein Expression and Antibody Preparation

Briefly, *nxhl* gene (zgc:113227, NM_001014319.2) was synthesized and the expression plasmid pET-B2m-*nxhl*-His was constructed using the seamless cloning technology (Figure S13 and Figure S14). The plasmid was transferred into the *Escherichia coli* strain B21 (DH3) for protein expression and the resulting protein was purified by Ni-NTA chromatography column. The purified *nxhl* protein was used to immunize Japanese big ear rabbits to produce polyclonal antibody. The specificity of polyclonal antibody was detected by anti-His Western blotting and its immunity was verified by ELISA. We purified 6mg of fusion protein (62.0 kDa) with 85% purity. After immunization in rabbits，a *nxhl* polyclonal antibody with a titer of 1:256,000 was obtained. The concentration of the *nxhl* antibody purified by Protein G affinity chromatography column was 10 mg/mL and the purity was 90%. The obtained *nxhl* antibody was used to perform Western blotting assays.

Western Blotting Assays

Zebrafish tissues from knock-down group and control were treated with 1 mL of tissue lysate (50 mmol/L Tris, 0.1% SDS,150 mmol/L NaCl, 1% NP-40, 5 mmol/L EDTA, 5 μg/mL aprotinin and 2 mmoL/L PMSF followed by lysis with protein lysate at 4°C for 30 min). All of the samples were centrifuged at 12,000 r/min at 4°C for 20 min and the supernatant was removed to detect the protein concentration using a bicinchoninic acid (BCA) kit (CWBIO. Co., Ltd., Shanghai, China). Samples were resolved by SDS-PAGE using a NuPAGE 4–12% gel (Life Technologies). Proteins were transferred onto a nitrocellulose filter (BioRad, Hercules, CA, USA) and sealed at 4°C overnight by 5% dried skimmed milk. The membranes were incubated with diluted primary rabbit polyclonal *ptprb* (VE-PTP)(PA5-68309, Invitrogen, USA) (1:1000), Hey2(PA5-72676, Invitrogen, USA) (1：2000), Dot1L(ab72454, Abcam, UK) (1:2000) , S1pr1(PA5-72648, Invitrogen, USA) (1：1000), HAND2 (PA5-68502, Invitrogen, USA) (1ug/mL) , Nucleolin (ab50279, Abcam, UK) (1:1000), Nucleolin (phosphor T76, ab168363, Abcam, UK) (1:1000), Nucleolin (phosphor T84, ab196338, Abcam, UK) (1:1000), Nucleolin (acetyl K88, ab196345, Abcam, UK) （1:1000), *nxhl* (Lab made, 1:1000) and *ptprb* (Lab made, 1:1000) antibodies overnight at 4°C followed by washing with PBS at room temperature. The membranes were treated with goat-anti-rabbit, rabbit-anti-goat or goat-anti-mouse IgG-HRP secondary antibody (1: 2000, CWBiotech., Ltd., Beijing, China) and incubated at 37°C for 2 h. After washing with PBS, the membrane was soaked in enhanced chemiluminescence (ECL) kit (CW Biotech., Ltd., Beijing, China) according to the manufacturer's protocols.

RNA Binding Protein Immunoprecipitation Assay (RIP)

To detect the interactions between *nxhl* mRNA and nucleolin protein, and VE-PTP mRNA and nucleolin protein, RIP was conducted as follows: constructed *nxhl*-pcDNA3.1 (pcDNA3.1 vector V79020, Invitrogen,

USA) was transferred into 293T cells and its overexpression was verified by qPCR. Then 10^7 293T cells were suspended and lysed for 20 mins with 1 ml RIPA lysis buffer (Thermo Fisher Scientific, USA) containing 1 μl of protease inhibitor (Beyotime, China). Twenty μl of cell lysates were used as input, for the IgG and IP experimental group. Magnetic beads were pretreated with an anti-rabbit IgG (Beyotime, China; negative control) or anti-Nucleolin (ab50279, Abcam, UK) for 1 h at room temperature, and cell extracts were immunoprecipitated with the beads-antibody complexes at 4℃ overnight.The retrieved RNA was purified by using the phenol-chloroform method and subjected to real-time qPCR and general reverse-transcription PCR for *nxhl* and VE-PTP analysis. Primers are list in Table S28.

RNA Pull-down Assay

To detect the interactions between VE-PTP mRNA and nucleolin protein in 293T cells, and *ptprb* mRNA and nucleolin protein in zebrafish tissues, probes for VE-PTP (human) and *ptprb* (zebrafish) were designed and synthesized. Probes were list in Table S28. Probes are labeled with 3 μg biotin then heated at 95℃ for 2 min followed by standing at room temperature for 30 min. Magnetic beads were washed and resuspended in 50 μl RIP buffer, then the biotinylated and denatured probes were added and incubated for 1 h at room temperature. The nucleolin protein was extracted with 1 ml RIP buffer, sonicated, centrifuged at 12,000 rpm for 15 min, and the supernatant (nucleolin protein) was retained. A magnetic separator was used to remove the liquid and the protein solution was rinsed three times using RIP buffer. The protein solution was added to the magnetic bead-probe mixture, and RNase inhibitor was added to the lysate.The mixture was incubated at room temperature for 1 h and washed five times with 1 ml RIP buffer once. Then 2×SDS loading buffer was added to the mixture, denatured at 95℃ for 10 min, and used for subsequent Western blotting. The Western blotting was performed as described above. The antibody Nucleolin (ab50279, Abcam, UK) (1:1000) was used in the detection of VE-PTP (human) and *ptprb* (zebrafish) in 293T cells and zebrafish tissue.

Statistical Analysis

All data are presented as mean ± SEM. Statistical analysis and graphical representation of the data were performed using GraphPad Prism 7.0 (GraphPad Software, San Diego, CA). Statistical evaluation was performed by using a Student's t test, ANOVA, or χ^2 test as appropriate. p value of less than 0.05 was considered statistically significant. Statistical significance is indicated by * or p value. * represents $p < 0.05$, and *** indicates $p < 0.0001$. The results are representative of at least three independent experiments.

RESULTS

WGD Drives Teleost Karyotypes Stability in Embryo

We have been thinking that whether the reserved genes after WGD in vertebrate function in regulation of angiogenesis. We tried to find such gene conserved in vertebrate. We used a teleost golden pompano which underwent WGD as an experimental model. We firstly obtained a high-quality genome by *de novo* sequencing, assembling and annotation of this teleost (Figure S1, S2, S3; TableS1-S17). The genomic landscape of genes, repetitive sequences, genome map markers, Hi-C data, and GC content of the golden pompano genome is visualized by circus [45] in Figure 1A. Then, we reconstructed the evolutionary history of teleost fishes with spotted gar, zebrafish and other teleosts to examine the evolutionary position of the teleost in vertebrate (Figure 1B, Figure S4). Assuming a constant rate of distribution of silent substitutions (dS)[46] of 1.5e-8, we revealed the dates of WGD (Ts3R) and Ss4R at 350 Mya and 96 Mya, respectively (Figure 1C). Genome collinearity comparison (Figure 1D, and Table S18) implied that teleost-ancestral karyotypes are considerably conserved in post-Ts3R rediploidization with large fissions, fusions or translocations (Figure 1E, and Table S19-S20). Next, we classified the Ts3R subgenomes according to the integrity of gene as belonging to the LF, MF, and Other subgenome.[47] The component of rediploidization-driven subgenomes

is unequally distributed among subgenomes (Figure 2A), suggesting an asymmetric retention of ancestral subgenomes in teleosts.[48, 49] For now, knowledge on the relationship between rediploidization process and embryo development stability is largely unclear. We then compared the genome-wide transcriptional levels of LF, MF, and Other karyotypes from whole-embryo development stages (OSP to YAPS) (Figure 2B). Karyotypes-retained regions (LF and MF) showed comparable expression levels during the embryo development, while karyotypes-loss regions (Other) were expressed at significantly lower levels (signed-rank sum test, $P < 0.01$) (Figure 2B, Figure S5). The Ks/Ks values of karyotypes-retained regions are significantly lower than those of karyotypes-loss regions (Figure 2C). This observation indicated that karyotypes-loss genes evolved faster than did the karyotypes-retained regions. We propose that karyotypes-retained genes are crucial for retaining embryo development stability and that karyotypes-loss genes are more prone to contribute to genetic diversity. Detail descriptions about subgenome and evolution can be found in supplementary information.

Nxhl Is A Conserved Homologue of *Nxh* Retained after WGD

Then we analyzed the gene expression pattern of golden pompano embryo (Figure S6 and Table S21-S26), and found that all 57 of the samples were separated into two components (Figure S6). The first 33 samples (from OSP to MGS) cluster into a clade and the residual 24 samples (from LGS to YAPS) cluster into another. The genes in the first clade were non-redundant reserved hub-genes and clearly “silenced” compared with those of the second clade, in which the gene levels show an explosive increase. We also noticed that before LGS, a group of genes in three stages, HBS, EGS, and MGS, are highly expressed in the first clade (Figure S6). We clustered these genes by using the WGCNA R package and found that most of them clustered into the purple_module and are co-expressed in a close network, indicating regulatory roles for these genes (Figure 2 DE). Among them, EVM0008813 (designated as New XingHuo, *nxh*; Figure 2F)

353 is retained one copy after WGD and dominantly expresses in HBS, EGS and MGS stages. It is closely co-
354 expressed with some key genes (Figure 2E), such as eomesa, dkk2 and mixl1, which play essential roles on
355 embryo development.[50-52] We purposed that *nxh* could be a crucial controller that regulates key steps of
356 embryo development. We found that *nxh* contains 3 exons with two introns and its expression (qPCR) in
357 EGS, MGS and LGS is highly identical to our sequencing data (FPKM, Figure 2F). We noticed that *nxh* is a
358 WGD-specific gene and belongs to the karyotypes-retained genes (MF), implicating its important conserve
359 function during evolution. We then searched its homologene in NCBI database by BLASTp and only one
360 gene *zgc:113227* (designated as New XingHuo-like; *nxhl*) shares 54.7% similarity to *nxh* at the amino acid
361 level in zebrafish. Also, the collinear analysis confirmed *nxhl* as its homologue gene in zebrafish (Figure
362 2G). We found that *nxh* and *nxhl* have the same functional domain DDE_Tnp_4 as the other seven genes in
363 different species have (Figure 2H), suggesting they may have similar biological functions during embryo
364 development. So, we asked what could the function of *nxhl* be?
365
366 **_Nxhl_ Affects Angiogenic Phenotypes _In Vitro_ and _In Vivo_**
367 Firstly, we investigated whether loss of *nxhl* affects morphology development in zebrafish. We observed that
368 both *nxhl* ^{e1i1} and *nxhl* ^{ATG} morphants resulted in nearly identical phenotypes of pericardial oedema, body
369 axis bending, and caudal fin defects (Figure 3A, Figure S7, and Figure S8) at 3 days post fertilization (dpf),
370 confirming that the phenotype of *nxhl* knockdown is *nxhl*-specific (Figure 3A). Regarding the vascular
371 system, embryos injected with *nxhl* ^{e1i1} MO present thinner ISVs (yellow arrows) and ectopic sprouts
372 (asterisk) of dorsal aorta compared with controls, and the *nxhl* knockdown prevents the parachordal vessel
373 (PAV) formation, the precursor to the lymphatic system. Moreover, heartbeat and circulation in the caudal
374 vein (CV) is visible in the control fish, but is abnormal in *nxhl*-MO-injected fish (Supplementary Movie1,
375 2). Both *nxhl* ^{e1i1} and *nxhl* ^{ATG} morphants dramatically disrupted normal splicing of *nxhl* (Figure 3A),

indicating high efficiency and specificity of the morpholino knockdown of *nxhl*. Consistent with this, *nxhl* morphants resulted in a high percentage of embryos with defects (81.55%, n=103 embryos in *nxhl* ^{e1i1} MO and 100%, n=106 embryos in *nxhl* ^{ATG} MO) and low survival rate (45.78%, n=225 embryos in *nxhl* ^{e1i1} MO and 17.68%, n=198 embryos in *nxhl* ^{ATG} MO) compared with controls (n=218 embryos) at 3 dpf (Figure 3A and Figure S7B). This confirmed that knockdown of *nxhl* certainly causes morphological defects in the heart and caudal fin in zebrafish.

We then used the *Tg(fli1a:EGFP)*^{y1} zebrafish as a model to investigate the connections between the vascular system and these phenotypes. Embryos were injected with 4 ng control MO or *nxhl* ^{e1i1} MO. We found that loss of *nxhl* caused intersegmental vessel (ISV) growth defect and disruption of the honeycomb structure in the CVP at 52 hpf (Figure 3B). Also, *nxhl* ^{e1i1} morphant resulted in a thinner ISV growth and ectopic sprouts of dorsal aorta at the rear-somite with only 10% of complete ISVs (n=365 embryos) compared with 98% of complete ISVs in controls (n=335 embryos). We observed that the *nxhl* knockdown prevented the PAV formation (Figure 3B) and caused specific defects in CVP formation (Figure 3C). Quantification of loop formation and the area at CVP showed a 8.2-fold and 3-fold decrease in *nxhl* ^{e1i1} morphants (n=10 embryos) at 52 hpf, respectively (Figure 3C). Our data indicate that *nxhl* plays a critical role in controlling PAV, ISV and CVP formation and vascular integrity during angiogenesis, which is an explanation strongly consistent with the heart and caudal fin phenotypes observed. What is the mechanism behind?

Endothelial cells (ECs) line the inner lumen of vessels and are the building elements of blood vessels, we then speculated that *nxhl* may affect angiogenesis via ECs. This is supported by the significant enrichment of the genes involved in blood vessel morphogenesis when *nxhl* was knocked down (Table S29). Since human Harbi1 gene shares DDE_Tnp_4 domain with *nxhl* (Figure 2E), it is supposed that both genes play similar roles. We used human umbilical vein endothelial cells (HUVECs) as a vascular epithelioid cells

399 model *in vitro*. Next, we designed siRNAs targeting human Harbi1, transferred siRNA into HUVECs and
400 investigated their cell migration, invasion, and tube formation. Silence of Harbi1 significantly inhibited the
401 tube formation and cell migration compared with controls (Figure 3D). Furthermore, the invasion abilities
402 in Harbi1 defect cells are also significantly inhibited compared with controls (Figure 3D). Moreover, silence
403 of Harbi1 significantly inhibited the angiogenesis of non-small cell lung cancer cell (A548) and human colon
404 cancer cell (HCT116) *in vitro* (Figure S9). This highlights the pro-angiogenesis function of Harbi1 and
405 indicates that *nxhl* like their human homolog Harbi1, play role in angiogenesis and anti-cancer process via
406 ECs.
407
408 **_Nxhl_ Regulates _Ptprb_ Expression and Angiogenic Networks**
409 To investigate how *nxhl* mediates angiogenesis, we firstly examined transcriptome sequencing (RNA-seq)
410 data from zebrafish after injection of 4 ng *nxhl* ^{e1i1} MO at 3 dpf. We found that loss of *nxhl* greatly changes
411 the transcriptome with 1955 down-regulated and 698 up-regulated (Figure S10; Table S21). We noticed that
412 in the KEGG pathways associated with angiogenesis development are significantly enriched in the *nxhl*-
413 silenced group (Figure S11; Table S22-26). We speculated that the transcription of genes linked to
414 angiogenesis development may also be significantly changed in the *nxhl*-silenced zebrafish. We then
415 screened and examined the expression of 18 genes that previously documented to be closely related to heart
416 defects and/ or angiogenesis.[53-57] Consistent with the RNA-seq data, we found that 13 of these genes (*ptprb*,
417 *tie2*, *nr2f1a*, *s1pr1*, *hey2*, *dot1L*, *hand2*, *erbb2*, *klf2a*, *mef2cb*, *mef2aa*, *ephB2a* and *cx40*.8) were significantly
418 decreased while two genes (*vegfaa and vegfr2*) increased sharply. *S1pr2, egfl7, and nrg2a* were kept
419 unchanged (Figure 4A-D). Notably, the arterial marker *ephB2a* and venous marker *erbb2* were decreased in
420 *nxhl* morphants compared to the wild-type (Figure 4D). Normally, the increase of v*egfaa and vegfr2* is linked
421 to the enhancement of vascular system.[58, 59] However, in our study, both genes increased while others

decreased when *nxhl* was silenced. We speculated this is a consequence of a negative feedback regulation to avoid an excessive decrease in the vascular system. We found that *nxhl* ^{e1i1} morphants result in decrease of the *nxhl* at protein level. *Ptprb*, the most decreased gene at mRNA level, is also greatly reduced at the protein level. The s1pr1, hand2, dot1L, and hey2 proteins were also downregulated compared with controls (Figure 4E). As previously reported, *ptprb, tie2, nr2f1a, s1pr1, vegfaa* and *vegfr2* normally contribute to vascular development and deletion of each of them leads to defects on the vascular system during embryo development,[14, 58-61] while loss of *dot1L, hand2, erbb2, mef2cb, mef2aa, ephB2a* or *cx40.8* always results in angiogenesis system or heart development defects.[55, 62-68] *Hey2 and klf2a* have been implicated in the regulation of both angiogenesis and heart development.[69, 70] Based on these reports, we built a schematic diagram of the network as shown in Figure 4F. This network demonstrates that silence of *nxhl* does downregulate the key genes that are essential for heart and /or vascular development. To this end, our results showed that loss of *nxhl* greatly affects the expression of these key genes in the network, suggesting that the heart and vascular phenotypes caused by *nxhl* deletion are greatly due to the regulation of these genes, and the expression profiles of these genes explain the *nxhl* deficient-induced phenotypes. Thus, we then asked how *nxhl* controls the angiogenesis and angiogenic networks.

Loss of *Ptprb* Duplicates the Phenotypes of *Nxhl* Deficiency

As described above, we noticed that *ptprb* is the most downregulated gene after silence of *nxhl* and is the one that closely linked to both vascular integrity and angiogenesis as well.[11, 13, 19, 71-73] To test whether there is a positive connection between *nxhl* and *ptprb,* we silenced *ptprb* by injection of 4 ng *ptprb* ^{e4i4} and *ptprb* ^{ATG} morphants designed (Figure S12, Table S30). Both *ptprb* morphants resulted in slight pericardial edema, shortened body axis and severe body axis bending in zebrafish (Figure 5A；Figure S12). Moreover, heartbeat and circulation in the caudal vein (CV) is visible in the control fish (Supplementary Movie 3,4), but is

abnormal in *ptprb*-MO-injected fish (Supplementary Movie 5-8). *Ptprb* morphants also resulted in a high percentage of embryos with defects (75.48%, n=208 embryos in *ptprb* MO and 0.94%, n=212 embryos in control) and lower survival rate compared with controls at 50 hpf (Figure 5A). Both *ptprb* morphants dramatically disrupted normal splicing of *ptprb* (Figure 5B-D), decreased the survival rate, but unchanged the *nxhl* expression, indicating high efficiency and specificity of the morpholino knockdown of *ptprb*. In the vascular system, loss of *ptprb* leads to an indefinite absence or deformity of DLAVs (blue arrowhead) and ISVs in the tail end (white and yellow arrowhead), and a decrease of PAV (red arrowhead) formation (Figure 5E). Knockdown of *ptprb* caused significantly decrease of the mean diameter of ISVs compared with controls (Figure 5F). Also, *ptprb* morphants caused CVP sinus cavities defects (Figure 5G), and resulted in a 5.6-fold and 2.2-fold decrease of CVP loop formation and CVP area (n=83 embryos) at 50 hpf, respectively (Figure 5G). These data are to some extent consistent with previous reports[57] and strongly suggest that loss of *ptprb* phenocopies *nxhl* deficiency. Moreover, We found that most of the 15 genes in *ptprb*-knockdown experiment present an expression profile similar to that in *nxhl*-knockdown experiment, except vegfaa and vegfr2 (Figure 5H). To this end, we logically concluded that knockdown of *ptprb* mimics phenotypes of *nxhl* deficiency, and both should act in the same signaling pathway. However, which one is downstream of the other is unclear. Therefore, we examined the *nxhl* expression after silence of *ptprb*, and we found that it was kept unchanged (Figure 5D), but we observed a significant decrease of *ptprb* expression after silence of *nxhl*. This confirms that *ptprb* acts at the downstream of *nxhl*.

Nxhl Regulates VE-PTP (*ptprb*) through Interactions with NCL

As mentioned above, among the 18 genes associated with heart and vascular development, 15 genes were significantly changed by both *nxhl* and *ptprb* morphants. We suppose these genes may be part of a regulatory network of their own. We then built a schematic diagram of the network according to previous reports (Figure

4F). This network presents connections between most of these genes, suggesting a cooperative regulation mechanism on the heart and vascular development. As we already knew that *ptprb* acts downstream of *nxhl*, we next asked if *nxhl* directly interacts with *ptprb* to mediate these genes. Thus, we designed *nxhl* probes and conducted a ChIRP-MS experiment in zebrafish to find out those proteins binding to *nxhl*. Eleven proteins with change folds above 2 were discovered (Figure 6A). This indicates that the *nxhl* RNA may interact with these proteins. Unexpectedly, *ptprb* was not found in these proteins (Figure 6A). This suggests that proteins other than *ptprb* may interact with *nxhl*. We next focused on the proteins that are associated with the vascular system, and nucleolin (NCL) (Figure 6A) aroused our interest because of its molecular conservation and important functions on angiogenesis.[31, 74] Loss of NCL in zebrafish causes oedema and body axis bending,[75] as well as suppression of adhesion, proliferation and migration of HUVECs.[76] These phenotypes are identical to the phenotypes caused by *nxhl* depletion, suggesting NCL may associate with *nxhl*. To figure out whether *nxhl* interacts with NCL, we performed RNA Immunoprecipitation (RIP) using the NCL protein as bait protein in 293T cells (Figure S13, S14, S15) and then detected the *nxhl* RNA using qPCR. We found that *nxhl* RNA is significantly higher than that in IgG control in the RNAs pulled-down by the NCL protein (Figure 6B). The RNA pulled down was amplified and the sequencing results confirmed that it is *nxhl* mRNA. This indicates that the NCL protein reversely interacts with *nxhl* RNA. Therefore, these experiments prove that *nxhl* RNA and NCL protein interact physically.

However, still no evidence was found on the interaction between *nxhl* and *ptprb*. Could it be that NCL interacts with *ptprb,* thus bridging *nxhl* and *ptprb?* Such scenario was never proposed or documented before. However, a report showed that VEGF interacts with NCL.[77] As *nxhl* acts similarly to VEGF on angiogenesis development, we then supposed that NCL might also interact with *ptprb* or its human homologue VE-PTP, the key molecule in angiogenesis. To test this hypothesis, we detected VE-PTP mRNA using the same RNAs pulled-down by NCL protein, and we found that VE-PTP mRNA is significantly higher than that in IgG

491 control. The RNA pulled down was amplified and the sequencing results proved that it is VE-PTP mRNA.
492 This confirms that the NCL protein can also interact with VE-PTP mRNA physically (Figure 6B). We next
493 verified this interaction in 293T cells using the VE-PTP RNA pulldown experiment in the reverse way, and
494 the result of western blotting against NCL protein supports the existence of interaction between VE-PTP and
495 NCL (Figure 6C). However, whether this interaction occurs between NCL and *ptprb* in zebrafish is unclear.
496 We next designed a zebrafish *ptprb* gene-specific probe to pull down the proteins that interact with *ptprb* in
497 the juvenile zebrafish. We found that the NCL protein strongly binds with *ptprb* (Figure 6C). These results
498 indicate that the NCL protein not only interacts with VEP-PTP in 293T cells but also with *ptprb* in zebrafish.
499 So far, we proved that *nxhl* and NCL, NCL and VEP-PTP (*ptprb*) interact physically. However, how
500 *nxhl* regulates NCL and *ptprb* is unclear. To address this issue, we micro-injected 4 ng *nxhl*-e1i1-MO in one
501 cell stage embryo, and found that resemble phenotypes were induced as that shown in Figure 3AB and Figure
502 S16. Meanwhile, we found that loss of *nxhl* not only causes a significant decrease of NCL mRNA and total
503 protein level but also leads to decrease of phosphorylated T76 and increase of the acetylated K88 of the NCL
504 protein (Figure 6D). This suggests that knockdown of *nxhl* significantly affects the expression of NCL, which
505 plays vital functions in angiogenesis,[31] although the impact of phosphorylation and acetylation of NCL
506 protein on the heart and vascular development have not been deeply understood yet.[74] Then we investigated
507 the expression of the downstream gene *ptprb*, and found that loss of *nxhl* also decreases *ptprb* at both mRNA
508 and protein levels (Figure 6D). These results suggest that silence of *nxhl* leads to angiogenesis defects due
509 to the downregulation of both NCL and *ptprb* via the interactions of *nxhl*-NCL and NCL-*ptprb*, which
510 consequently mediates the angiogenesis-linked landmark gene network.
511
512 **NCL Regulates Angiogenesis and VE-PTP *in vitro***
513 Although the physical interactions between *nxhl* and NCL and NCL and *ptprb* (VE-PTP) and regulatory role

of *nxhl* on NCL and *ptprb* (VE-PTP) are confirmed in our study, whether NCL regulates *ptprb* (VE-PTP) is still unknown. We next examined the functions of NCL on angiogenesis and expression of VE-PTP by silence of NCL in HUVECs. As shown in Figure 7, silence of NCL not only significantly inhibited the tube formation but also the cell migration of HUVECs comparing with the controls. Notably, silence of NCL greatly decreased the expression of VE-PTP at both mRNA and protein levels, suggesting that NCL not only interacts with VE-PTP but also regulates its expression. This highlights the pro-angiogenesis function of NCL and its direct regulatory role on VE-PTP expression, and proves that the *nxhl*-NCL-VE-PTP (*ptprb*) signaling pathway is logical and reasonable for angiogenesis.

Nxhl Controls Angiogenesis by Targeting VE-PTP (*ptprb*)and Linking Angiogenesis Regulatory Genes

It is confirmed that loss of *nxhl* not only downregulates *ptprb* but the angiogenesis landmark genes (Figure 4F), with the addition of finding that *nxhl* binds to NCL which interacts with VE-PTP (*ptprb*), we conclude that *nxhl* controls angiogenesis through *nxhl*-NCL-VE-PTP (*ptprb*)-linked angiogenesis regulatory genes. This, for the first time, uncovers the existence of upstream regulatory genes of VE-PTP (*ptprb*). Based on these data, we built a new schematic diagram based on the network in Figure 4F that shows the novel *nxhl*-NCL-VE-PTP (*ptprb*) signaling links to the keystone angiogenesis genes (Figure 8A vs. Figure 4F). We also made a schematic diagram to describe the possible mechanism underlying *nxhl*-induced phenotypes of pericardial oedema and vascular patterning defects (Figure 8B). Knockdown of *nxhl* significantly and broadly downregulates angiogenesis-associated landmark genes, including d*ot1L, hand2, erbb2, mef2aa, n2rf1a, hey2, s1pr1, tie2, ptprb, meff2cb, ephB2a, klf2a and cx40.8*, through *nxhl*-NCL-VE-PTP (*ptprb*)pathway, while *vegfr2* and *vegfaa* negative feedback control this downregulation. Moreover, loss of *nxhl* increases the phosphorylation of NCL(T76) and decreases the acetylation NCL (K88), indicating that *nxhl* may control angiogenesis by impacting NCL posttranslational modification to regulate downstream VE-PTP signaling pathways. This highlights the crucial role of *nxhl* on angiogenesis development via a hitherto

538 unreported *nxhl*-NCL-VE-PTP (*ptprb*) pathway, which extends the upstream regulatory member of keystone
539 gene VE-PTP (*ptprb*). We conclude that *nxhl* controls angiogenesis by targeting VE-PTP (*ptprb*) through
540 interaction with NCL and linking vascular keystone regulatory genes. Given the extreme importance of the
541 angiogenesis development, and the broad connections with landmark genes, we believe the finding of this
542 novel signaling pathway to be of considerable importance for the study of the angiogenesis development and
543 angiogenesis-dependent diseases.
544

545 **DISCUSSION**

546 Previous studies showed that VE-PTP is a key player in regulation of angiogenesis and EC adherens
547 junction,[12-15] and is a potential therapeutic target for angiogenesis-dependent diseases.[7, 8] It binds to some
548 proteins, such as Tie2, VEGFR2, VE-cadherin and FGD5, that mediate angiogenic signaling pathways.[18, 25-
549 27, 29] In the present study, we identified a novel zebrafish gene *nxhl*. It controls angiogenic processes *in vitro*
550 and *in vivo*. Deletion of *nxhl* causes angiogenesis-associated phenotypes. Loss of VE-PTP duplicates the
551 phenotypes caused by the upstream *nxhl* deficiency, confirming both act in the same angiogenic signaling
552 pathway. We for the first time show that *nxhl* physically binds to NCL which interacts with VE-PTP and
553 thereby controls angiogenesis. Our study defines a novel *nxhl*-NCL-VE-PTP signaling pathway for
554 angiogenesis regulation.

555 Anti-angiogenic drugs have been a focus of study and lots of inhibitors of angiogenesis are currently
556 used as monotherapy or in combination with chemotherapy or cytokine treatment.[78] Previous studies showed
557 that AKB-9778, a specific inhibitor of VE-PTP, has demonstrated promising clinic perspective for treatment
558 of angiogenesis-dependent diseases, although it is still under clinical investigation.[31-34] This highlights the
559 great value of VE-PTP on anti-angiogenic agents. Logically, targeting the upstream regulator of VE-PTP
560 may achieve the same or better effects to that of AKB-9778, because its broader and stronger modulatory
561 forces. However, few upstream regulation mechanisms of VE-PTP has been documented yet. In this study,

562 we identify *nxhl* as a novel powerful upstream regulator of VE-PTP. We find that *nxhl* plays a role in
563 angiogenesis not only because it sharply decreases expressions of VE-PTP and other key angiogenic genes,
564 but also the *nxhl* deletion-caused angiogenesis phenotypes, such as pericardial oedema, defects of caudal fin,
565 intersegmental vessel and caudal vein plexus, are duplicated by the VE-PTP deficiency. These phenotypes
566 of VE-PTP knockdown are mostly identical to a previous study using different morphants to ours.[57]
567 Additionally, no changes occur in *nxhl* expression upon VE-PTP knockdown, but the expression of VE-PTP
568 significantly decreases upon loss of *nxhl*. This highly implicates that *nxhl* regulates VE-PTP at its upstream
569 and both act in a same signaling pathway. Importantly, the splice-blocking *nxhl* MO displayed phenotypes
570 which are totally overlapping with the translation-blocking MOs, confirming the specificity of phenotypes
571 obtained by *nxhl* injection rather than MO off-target effects. Moreover, *nxhl* controls angiogenesis via ECs
572 migration and tube formation, which is consists with the angiogenic characteristics of VE-PTP on EC
573 adhesion and integrity,[16-18] confirming its angiogenesis controlling function acts via ECs. This is also
574 strongly supported by our findings that silence of the highly conserve human homologue of *nxhl* not only
575 inhibits the HUVECs migration and tube formation but suppresses the migrations and invasions of cancer
576 cell lines by inhibiting ECs (Figure S9). All these data suggest that *nxhl* is a powerful upstream angiogenesis
577 governor targeting VE-PTP.

578 On the other hand, the effects of *nxhl* controlling angiogenesis depend on its binding with NCL, which
579 simultaneously bridges *nxhl* and VE-PTP. To our best knowledge, this is the first description on the
580 interactions between *nxhl* and NCL, NCL and VE-PTP, uncovering a novel angiogenesis signaling complex
581 at the upstream of VE-PTP. NCL expresses broadly in all cells in a proliferation-dependent manner [79] and
582 almost all compartments of cells. Like VEP-TP, NCL also associates both cancer and other angiogenic
583 diseases. However, this function is more likely related to the cell surface NCL rather than that in other
584 compartments. The cell surface NCL is clustered and highly expressed in ECs of angiogenic blood vessels

585 during angiogenesis,[26, 27, 80] suggesting that NCL functions as an angiogenic gene. Also, it expresses at the
586 surface of tumor cells, including tumor cells and tumor vasculature. This allows the targeting of different
587 cellular compartments of solid tumors. Additionally, cell surface NCL has been identified in cancer stem
588 cells (CSCs) from different breast cancer cells lines.[81] Since CSCs are highly tumorigenic,[82, 83] the
589 association of NCL with the stemness highlights the value of NCL as a potential therapeutic target.[84]
590 Importantly, dysregulation of NCL associates with higher risk of recurrence or poorer overall survival for
591 some cancers.[85] These define NCL as both prognostic marker and therapeutic target, highlighting its great
592 value on development of anti-angiogenic drugs.[31, 74] In this study, we identified the direct interactions
593 between *nxhl* and NCL, and NCL and VE-PTP (*ptprb*) in both zebrafish and 293T cells by ChIRP, RNA
594 Immunoprecipitation and RNA pulldown methods, although we did not yet figure out which subset of NCL
595 (surface, nucleolar or cytoplasmic NCL) participates in this interaction. Importantly, we proved that silence
596 of NCL inhibits angiogenesis of HUVECs and expression of VE-PTP at both mRNA and protein levels. This
597 further supports that NCL plays key roles on angiogenesis by directly controlling downstream VE-PTP.
598 Moreover, deletion of *nxhl* causes a significant decrease of NCL at both mRNA and total protein levels,
599 suggesting that *nxhl* significantly affects and regulates the NCL. This is further supported by the decrease of
600 the phosphorylated T76 and increase of the acetylated K88 of NCL protein upon the *nxhl* knockdown (Figure
601 6D). Previous study suggested that NCL phosphorylation status heavily affects its cellular
602 compartmentalization.[86] It promotes EGFR phosphorylation, dimerization and cell growth.[28, 87] It also
603 promotes HER2 (namely Erbb2) phosphorylation and subsequent MAPK/ Erk pathway activation.[30]
604 Clinically, combination treatment with NCL and HER2 inhibitors exhibited superior efficacy compared with
605 single treatment in the invasion capacity of breast cancer cells.[88] Except EGF and HER2, NCL also binds to
606 VEGF,[26] whose receptor VEGFR2 is tightly associated with VE-PTP resulting in increase of VEGFR2
607 phosphorylation and activation.[19] Since EGFR, HER2 and VE-PTP/VEGFR2 have been tightly associated

608 with angiogenesis, we consider *nxhl* may control angiogenesis by affecting NCL phosphorylation which
609 regulates downstream EGFR, HER2 or VE-PTP/VEGFR2 signaling pathways. Notably, in our study,
610 expressions of VEGFR2 and Erbb2 are significantly affected by *nxhl* knockdown, partially supporting this
611 point of view. However, this needs to be investigated in our future works. In addition, NCL acetylation at
612 K88 was previously described *in vivo* and *in vitro*, and this post-translational modification sharply changes
613 its cellular localization. Previous study suggested that NCL may be involved in pre-mRNA synthesis or
614 metabolism because of the presence of NCL-K88ac in nuclear speckles.[89] However, the characterization and
615 functional significance of NCL acetylation in angiogenesis are still unclear. What the consequences of NCL-
616 K88ac increase on *nxhl* or VE-PTP and subsequent pathways needs further investigation. Taken together,
617 our data enabled us to conclude that *nxhl* regulates the angiogenesis via the *nxhl*-NCL-VE-PTP (*ptprb*)
618 pathway.

619 The strong power of *nxhl* on angiogenesis controlling also relies on the effects of some other crucial
620 downstream angiogenic genes (such as Tie2, VEGFaa, VEGFR2, S1pr1 and Hey2) which broadly associate
621 VE-PTP signaling (Figure 4, Figure 8). What needs to be stressed is that the expressions of these genes
622 explain the phenotypes induced by the *nxhl* deficiency. They all play irreplaceable roles in multiple aspects
623 of angiogenesis development. For instance, Hand2 is vital in heart development in zebrafish and mouse.[90,
624 91] It has been identified as a specifier of outflow tract cells in the mouse by single cell sequencing.[92] Hey2
625 mediates the dynamics of cardiac progenitor cells addition to the zebrafish heart.[69] It is identified as a
626 component of the NKX2-5 cardiac transcriptional network regulating the early stage of the human heart
627 development.[93] The Dot1L,[63] Mef2aa,[64] Mef2cb,[65] Erbb2,[66] Klf2a[70] and EphB2a[94] also play key roles in the
628 growth of the chamber, cardiomyocyte differentiation, myocardial cell addition, cardiac trabeculation, atrial
629 fibrillation, gap junction, valvulogenesis and myocardial trabeculation during heart development.
630 Importantly, the heart and vascular development are always linked. Previous studies showed that silence of

zebrafish S1pr1 not only leads to global and pericardial edema, lack of blood circulation, altered posterior cardinal vein structure, reduced vascularization in ISVs and CVPs,[61] but also regulates the endothelial barrier integrity via the S1pr1/VE-cadherin/EphB4a pathway.[95] Similar phenotypes can be induced by the knockdown of Nr2fla in zebrafish due to the decrease of cell proliferation and migration instead of cell death in ECs.[60] Moreover, mutation of Nr2f1a results in smaller atria due to a specific reduction in the atrial cardiomyocyte number and an increase of the rate of atrial cardiomyocyte differentiation.[96] Another key gene, Tie2, is essentially required for ISV growth, sprouting, migration, and proliferation of tip cells and acts coordinately with VEGF signaling to control angiogenesis *in vivo*.[97] Loss of Tie2 leads to death at E10.5 due to vessel remodeling defects and lack of trabeculation.[98] Notably, Ang-Tie2 system is indispensable for vascular and lymphatic development.[99] The anti-angiogenic effects of VE-PTP inhibitor, AKB-9778, likely rely on the Ang-Tie2 pathway.[17] In our study, *nxhl* deletion leads to significant decrease of Tie2, suggesting it regulates not only VE-PTP but also Ang-Tie2 system, which crosstalk with VE-PTP. From this point of review, *nxhl* is a multifunctional master of angiogenesis process. This explains our findings that the phenotypes induced by *nxhl* knockdown mostly resemble the phenotypes caused by deletion of these genes associate with VE-PTP. Although the specific mechanisms underlying need further elucidation, given the extreme importance of these genes in angiogenesis development, we consider the phenotypes caused by *nxhl* morphants as direct or indirect consequences of the down-regulation of VE-PTP and these key genes. We believe the fire-new *nxhl*-NCL-VE-PTP signaling pathway is a highlight for vertebrate angiogenesis development regulation.

In conclusion, we clearly demonstrate that a novel gene *nxhl* controls angiogenesis by targeting VE-PTP through interaction with NCL whose posttranslational modification (phosphorylation and acetylation) may affect downstream VE-PTP signaling pathways. Furthermore, we have elucidated some of the crucial downstream pathways that may be implicated in regulating the angiogenesis. This study reveals a fire-new

nxhl-NCL-VE-PTP signaling pathway governing vertebrate angiogenesis development, implicating its great potential as therapeutic target for angiogenesis-dependent diseases.

Acknowledgements

We thank Mr Zhuanbin Wu for zebrafish analysis advices and technical consults.

Sources of Funding

This research was supported by the Guangxi science and technology major project (GuiKeAA18242031, GuiKeAA18242031-2, GuiKeAA17204080, GuiKe AA17204080-3), Guangxi Key Laboratory for Aquatic Genetic Breeding and Healthy Aquaculture, Guangxi Institute of Fishery Sciences (14-045-10 (14-A-01-02),15-140-23(15-A-01-01, 15-A-01-02, 15-A-01-03),16-380-38(16-A-01-01, 16-A-01-02), 17-259-29 and 19-A-01-05) and Guangxi research institutes of basic research and public service special operations (GXIF-2016-03, GXIF-2016-09, GXIF-2016-18, GXIF-2016-19).

Author contributions

H.L.L and X.H.C designed the scientific objectives and oversaw the project. H.L.L., X.H.C., Y.Z.Z., J.X.P., and Y.L discussed the primary ideas of the article. Y.D.Z, J.X.P., Y.L., Y.H., Q.Y.L., P.P.H., C.L.Y., P.Y.W., X.L.C., and P.F.F. collected samples for sequencing DNA and RNA. C.M.J. and their colleagues performed genome sequencing, assembly and annotation. C.M.J. and H.Y.Y performed phylogenomic and whole genome duplication evolution analysis. C.M.J. H.Y.Y., H.L.L., and Y.D.Z performed RNA-seq analysis. H.L.L and Y.D.Z performed functional assay of zebrafish *nxhl* gene and Harbi1 gene. C.M.J, H.Y.Y., H.L.L., and Y.D.Z prepared the supplemental data and method. C.M.J. and H.L.L prepared the draft manuscript with input from all other authors. H.L.L., X.H.C., Y.L., and H.K.Z. discussed and revised the manuscript.

Data availability

The authors declare that all data reported in this study are fully and freely available from the date of publication. This Whole Genome Shotgun project has been deposited at DDBJ/ENA/GenBank under the accession WOFJ00000000. The version described in this paper is version WOFJ01000000. The draft genome data (genome assembling and annotations) and RNA-Seq data of the embryo are available under BioProject PRJNA574895. Transcriptome (Illumina) data of *nxhl* silence are available in the Sequence Read Archive (SRA) with accession number SRR10199007 and SRR10199008 under BioProject PRJNA573544 .

Disclosures

The authors declare no competing financial interests.

Supplemental material

Supplemental Information (Notes and Methods)

Supplemental Figures (Figure S1-S16)

Supplemental Tables (Table S1-S28)

Supplemental videos (Movie 1-8)

REFERENCES

1. Handa JT, Bowes Rickman C, Dick AD, Gorin MB, Miller JW, Toth CA, Ueffing M, Zarbin M and Farrer LA. A systems biology approach towards understanding and treating non-neovascular age-related macular degeneration. *Nat Commun*. 2019;10:3347.

2. Diabetic Retinopathy Clinical Research N, Wells JA, Glassman AR, Ayala AR, Jampol LM, Aiello LP, Antoszyk AN, Arnold-Bush B, Baker CW, Bressler NM, Browning DJ, Elman MJ, Ferris FL, Friedman SM, Melia M, Pieramici DJ, Sun JK and Beck RW. Aflibercept, bevacizumab, or ranibizumab for diabetic macular edema. *N Engl J Med*. 2015;372:1193-203.

3. Smolen JS, Landewe RBM, Bijlsma JWJ, Burmester GR, Dougados M, Kerschbaumer A, McInnes IB, Sepriano A, van Vollenhoven RF, de Wit M, Aletaha D, Aringer M, Askling J, Balsa A, Boers M, den Broeder AA, Buch MH, Buttgereit F, Caporali R, Cardiel MH, De Cock D, Codreanu C, Cutolo M, Edwards CJ, van Eijk-Hustings Y, Emery P, Finckh A, Gossec L, Gottenberg JE, Hetland ML, Huizinga TWJ, Koloumas M, Li Z, Mariette X, Muller-Ladner U, Mysler EF, da Silva JAP, Poor G, Pope JE, Rubbert-Roth A, Ruyssen-Witrand A, Saag KG, Strangfeld A, Takeuchi T, Voshaar M, Westhovens R and van der Heijde D.

EULAR recommendations for the management of rheumatoid arthritis with synthetic and biological disease-modifying antirheumatic drugs: 2019 update. *Ann Rheum Dis*. 2020;79:685-699.

4. Souilhol C, Serbanovic-Canic J, Fragiadaki M, Chico TJ, Ridger V, Roddie H and Evans PC. Endothelial responses to shear stress in atherosclerosis: a novel role for developmental genes. *Nat Rev Cardiol*. 2020;17:52-63.

5. Folkman J. Angiogenesis: an organizing principle for drug discovery? *Nat Rev Drug Discov*. 2007;6:273-86.

6. Grothey A and Galanis E. Targeting angiogenesis: progress with anti-VEGF treatment with large molecules. *Nat Rev Clin Oncol*. 2009;6:507-18.

7. Wilke H, Muro K, Van Cutsem E, Oh SC, Bodoky G, Shimada Y, Hironaka S, Sugimoto N, Lipatov O, Kim TY, Cunningham D, Rougier P, Komatsu Y, Ajani J, Emig M, Carlesi R, Ferry D, Chandrawansa K, Schwartz JD, Ohtsu A and Group RS. Ramucirumab plus paclitaxel versus placebo plus paclitaxel in patients with previously treated advanced gastric or gastro-oesophageal junction adenocarcinoma (RAINBOW): a double-blind, randomised phase 3 trial. *Lancet Oncol*. 2014;15:1224-35.

8. Ferrara N and Adamis AP. Ten years of anti-vascular endothelial growth factor therapy. *Nat Rev Drug Discov*. 2016;15:385-403.

9. Giantonio BJ, Catalano PJ, Meropol NJ, O'Dwyer PJ, Mitchell EP, Alberts SR, Schwartz MA, Benson AB, 3rd and Eastern Cooperative Oncology Group Study E. Bevacizumab in combination with oxaliplatin, fluorouracil, and leucovorin (FOLFOX4) for previously treated metastatic colorectal cancer: results from the Eastern Cooperative Oncology Group Study E3200. *J Clin Oncol*. 2007;25:1539-44.

10. Fachinger G, Deutsch U and Risau W. Functional interaction of vascular endothelial-protein-tyrosine phosphatase with the angiopoietin receptor Tie-2. *Oncogene*. 1999;18:5948-53.

11. Dominguez MG, Hughes VC, Pan L, Simmons M, Daly C, Anderson K, Noguera-Troise I, Murphy AJ, Valenzuela DM, Davis S, Thurston G, Yancopoulos GD and Gale NW. Vascular endothelial tyrosine phosphatase (VE-PTP)-null mice undergo vasculogenesis but die embryonically because of defects in angiogenesis. *Proc Natl Acad Sci U S A*. 2007;104:3243-8.

12. Baumer S, Keller L, Holtmann A, Funke R, August B, Gamp A, Wolburg H, Wolburg-Buchholz K, Deutsch U and Vestweber D. Vascular endothelial cell-specific phosphotyrosine phosphatase (VE-PTP) activity is required for blood vessel development. *Blood*. 2006;107:4754-62.

13. Hayashi M, Majumdar A, Li X, Adler J, Sun Z, Vertuani S, Hellberg C, Mellberg S, Koch S, Dimberg A, Koh GY, Dejana E, Belting HG, Affolter M, Thurston G, Holmgren L, Vestweber D and Claesson-Welsh L. VE-PTP regulates VEGFR2 activity in stalk cells to establish endothelial cell polarity and lumen formation. *Nat Commun*. 2013;4:1672.

14. Winderlich M, Keller L, Cagna G, Broermann A, Kamenyeva O, Kiefer F, Deutsch U, Nottebaum AF and Vestweber D. VE-PTP controls blood vessel development by balancing Tie-2 activity. *J Cell Biol*. 2009;185:657-71.

15. Monaghan-Benson E and Burridge K. VE-cadherin status as an indicator of microvascular permeability. *Methods Mol Biol*. 2013;1046:335-42.

16. Nawroth R, Poell G, Ranft A, Kloep S, Samulowitz U, Fachinger G, Golding M, Shima DT, Deutsch U and Vestweber D. VE-PTP and VE-cadherin ectodomains interact to facilitate regulation of phosphorylation and cell contacts. *EMBO J*. 2002;21:4885-95.

17. Nottebaum AF, Cagna G, Winderlich M, Gamp AC, Linnepe R, Polaschegg C, Filippova K, Lyck R, Engelhardt B, Kamenyeva O, Bixel MG, Butz S and Vestweber D. VE-PTP maintains the endothelial barrier via plakoglobin and becomes dissociated from VE-cadherin by leukocytes and by VEGF. *J Exp Med*. 2008;205:2929-45.

18. Vestweber D. Cadherins in tissue architecture and disease. *J Mol Med (Berl)*. 2015;93:5-11.

19. Mellberg S, Dimberg A, Bahram F, Hayashi M, Rennel E, Ameur A, Westholm JO, Larsson E, Lindahl P, Cross MJ and Claesson-Welsh L. Transcriptional profiling reveals a critical role for tyrosine phosphatase VE-PTP in regulation of VEGFR2 activity and endothelial cell morphogenesis. *FASEB J*. 2009;23:1490-502.

20. Shen J, Frye M, Lee BL, Reinardy JL, McClung JM, Ding K, Kojima M, Xia H, Seidel C, Lima e Silva R, Dong A, Hackett SF, Wang J, Howard BW, Vestweber D, Kontos CD, Peters KG and Campochiaro PA. Targeting VE-PTP activates TIE2 and stabilizes the ocular vasculature. *J Clin Invest*. 2014;124:4564-76.

21. Souma T, Thomson BR, Heinen S, Carota IA, Yamaguchi S, Onay T, Liu P, Ghosh AK, Li C, Eremina V, Hong YK,

Economides AN, Vestweber D, Peters KG, Jin J and Quaggin SE. Context-dependent functions of angiopoietin 2 are determined by the endothelial phosphatase VEPTP. *Proc Natl Acad Sci U S A*. 2018;115:1298-1303.

22. Li G, Sachdev U, Peters K, Liang X and Lotze MT. The VE-PTP Inhibitor AKB-9778 Improves Antitumor Activity and Diminishes the Toxicity of Interleukin 2 (IL-2) Administration. *J Immunother*. 2019;42:237-243.

23. Goel S, Gupta N, Walcott BP, Snuderl M, Kesler CT, Kirkpatrick ND, Heishi T, Huang Y, Martin JD, Ager E, Samuel R, Wang S, Yazbek J, Vakoc BJ, Peterson RT, Padera TP, Duda DG, Fukumura D and Jain RK. Effects of vascular-endothelial protein tyrosine phosphatase inhibition on breast cancer vasculature and metastatic progression. *J Natl Cancer Inst*. 2013;105:1188-201.

24. Liu WS, Wang RR, Sun YZ, Li WY, Li HL, Liu CL, Ma Y and Wang RL. Exploring the effect of inhibitor AKB-9778 on VE-PTP by molecular docking and molecular dynamics simulation. *J Cell Biochem*. 2019;120:17015-17029.

25. Campochiaro PA, Sophie R, Tolentino M, Miller DM, Browning D, Boyer DS, Heier JS, Gambino L, Withers B, Brigell M and Peters K. Treatment of diabetic macular edema with an inhibitor of vascular endothelial-protein tyrosine phosphatase that activates Tie2. *Ophthalmology*. 2015;122:545-54.

26. Christian S, Pilch J, Akerman ME, Porkka K, Laakkonen P and Ruoslahti E. Nucleolin expressed at the cell surface is a marker of endothelial cells in angiogenic blood vessels. *J Cell Biol*. 2003;163:871-8.

27. Fogal V, Sugahara KN, Ruoslahti E and Christian S. Cell surface nucleolin antagonist causes endothelial cell apoptosis and normalization of tumor vasculature. *Angiogenesis*. 2009;12:91-100.

28. Farin K, Schokoroy S, Haklai R, Cohen-Or I, Elad-Sfadia G, Reyes-Reyes ME, Bates PJ, Cox AD, Kloog Y and Pinkas-Kramarski R. Oncogenic synergism between ErbB1, nucleolin, and mutant Ras. *Cancer Res*. 2011;71:2140-51.

29. Koutsioumpa M and Papadimitriou E. Cell surface nucleolin as a target for anti-cancer therapies. *Recent Pat Anticancer Drug Discov*. 2014;9:137-52.

30. Wolfson E, Goldenberg M, Solomon S, Frishberg A and Pinkas-Kramarski R. Nucleolin-binding by ErbB2 enhances tumorigenicity of ErbB2-positive breast cancer. *Oncotarget*. 2016;7:65320-65334.

31. Huang Y, Shi H, Zhou H, Song X, Yuan S and Luo Y. The angiogenic function of nucleolin is mediated by vascular endothelial growth factor and nonmuscle myosin. *Blood*. 2006;107:3564-71.

32. Quiroz-Mercado J, Ramirez-Velazquez N, Partido G, Zenteno E, Chavez R, Agundis-Mata C, Jimenez-Martinez MC and Garfias Y. Tissue and cellular characterisation of nucleolin in a murine model of corneal angiogenesis. *Graefes Arch Clin Exp Ophthalmol*. 2016;254:1753-63.

33. Destouches D, Huet E, Sader M, Frechault S, Carpentier G, Ayoul F, Briand JP, Menashi S and Courty J. Multivalent pseudopeptides targeting cell surface nucleoproteins inhibit cancer cell invasion through tissue inhibitor of metalloproteinases 3 (TIMP-3) release. *J Biol Chem*. 2012;287:43685-93.

34. Gilles ME, Maione F, Cossutta M, Carpentier G, Caruana L, Di Maria S, Houppe C, Destouches D, Shchors K, Prochasson C, Mongelard F, Lamba S, Bardelli A, Bouvet P, Couvelard A, Courty J, Giraudo E and Cascone I. Nucleolin Targeting Impairs the Progression of Pancreatic Cancer and Promotes the Normalization of Tumor Vasculature. *Cancer Res*. 2016;76:7181-7193.

35. Jain N, Zhu H, Khashab T, Ye Q, George B, Mathur R, Singh RK, Berkova Z, Wise JF, Braun FK, Wang X, Patel K, Xu-Monette ZY, Courty J, Young KH, Sehgal L and Samaniego F. Targeting nucleolin for better survival in diffuse large B-cell lymphoma. *Leukemia*. 2018;32:663-674.

36. Romano S, Fonseca N, Simoes S, Goncalves J and Moreira JN. Nucleolin-based targeting strategies for cancer therapy: from targeted drug delivery to cytotoxic ligands. *Drug Discov Today*. 2019;24:1985-2001.

37. Danninger C and Gimona M. Live dynamics of GFP-calponin: isoform-specific modulation of the actin cytoskeleton and autoregulation by C-terminal sequences. *J Cell Sci*. 2000;113 Pt 21:3725-36.

38. Song HD, Sun XJ, Deng M, Zhang GW, Zhou Y, Wu XY, Sheng Y, Chen Y, Ruan Z, Jiang CL, Fan HY, Zon LI, Kanki JP, Liu TX, Look AT and Chen Z. Hematopoietic gene expression profile in zebrafish kidney marrow. *Proc Natl Acad Sci U S A*. 2004;101:16240-5.

39. Lawson ND and Weinstein BM. In vivo imaging of embryonic vascular development using transgenic zebrafish. *Dev Biol*. 2002;248:307-18.

40. Lyons MS, Bell B, Stainier D and Peters KG. Isolation of the zebrafish homologues for the tie-1 and tie-2 endothelium-

specific receptor tyrosine kinases. *Dev Dyn*. 1998;212:133-40.

41. Tran TC, Sneed B, Haider J, Blavo D, White A, Aiyejorun T, Baranowski TC, Rubinstein AL, Doan TN, Dingledine R and Sandberg EM. Automated, quantitative screening assay for antiangiogenic compounds using transgenic zebrafish. *Cancer Res*. 2007;67:11386-92.

42. Westerfield M. The Zebrafish Book: A Guide for the Laboratory use of Zebrafish. *Eugene: The University of Oregon Press* 1993.

43. Kimmel CB, Ballard WW, Kimmel SR, Ullmann B and Schilling TF. Stages of embryonic development of the zebrafish. *Dev Dyn*. 1995;203:253-310.

44. Nasevicius A and Ekker SC. Effective targeted gene 'knockdown' in zebrafish. *Nat Genet*. 2000;26:216-20.

45. Krzywinski M, Schein J, Birol I, Connors J, Gascoyne R, Horsman D, Jones SJ and Marra MA. Circos: an information aesthetic for comparative genomics. *Genome Res*. 2009;19:1639-45.

46. Crete-Lafreniere A, Weir LK and Bernatchez L. Framing the Salmonidae family phylogenetic portrait: a more complete picture from increased taxon sampling. *PLoS One*. 2012;7:e46662.

47. Cheng F, Mandakova T, Wu J, Xie Q, Lysak MA and Wang X. Deciphering the diploid ancestral genome of the Mesohexaploid Brassica rapa. *Plant Cell*. 2013;25:1541-54.

48. Emery M, Willis MMS, Hao Y, Barry K, Oakgrove K, Peng Y, Schmutz J, Lyons E, Pires JC, Edger PP and Conant GC. Preferential retention of genes from one parental genome after polyploidy illustrates the nature and scope of the genomic conflicts induced by hybridization. *PLoS Genet*. 2018;14:e1007267.

49. Liang Z and Schnable JC. Functional Divergence between Subgenomes and Gene Pairs after Whole Genome Duplications. *Mol Plant*. 2018;11:388-397.

50. Du S, Draper BW, Mione M, Moens CB and Bruce A. Differential regulation of epiboly initiation and progression by zebrafish Eomesodermin A. *Dev Biol*. 2012;362:11-23.

51. McGraw HF, Culbertson MD and Nechiporuk AV. Kremen1 restricts Dkk activity during posterior lateral line development in zebrafish. *Development*. 2014;141:3212-21.

52. Hart AH, Hartley L, Sourris K, Stadler ES, Li R, Stanley EG, Tam PP, Elefanty AG and Robb L. Mixl1 is required for axial mesendoderm morphogenesis and patterning in the murine embryo. *Development*. 2002;129:3597-608.

53. Pereira CF, Chang B, Gomes A, Bernitz J, Papatsenko D, Niu X, Swiers G, Azzoni E, de Bruijn MF, Schaniel C, Lemischka IR and Moore KA. Hematopoietic Reprogramming In Vitro Informs In Vivo Identification of Hemogenic Precursors to Definitive Hematopoietic Stem Cells. *Dev Cell*. 2016;36:525-39.

54. Boselli F, Freund JB and Vermot J. Blood flow mechanics in cardiovascular development. *Cell Mol Life Sci*. 2015;72:2545-59.

55. Hinits Y, Pan L, Walker C, Dowd J, Moens CB and Hughes SM. Zebrafish Mef2ca and Mef2cb are essential for both first and second heart field cardiomyocyte differentiation. *Dev Biol*. 2012;369:199-210.

56. Ruiz-Herguido C, Guiu J, D'Altri T, Ingles-Esteve J, Dzierzak E, Espinosa L and Bigas A. Hematopoietic stem cell development requires transient Wnt/beta-catenin activity. *J Exp Med*. 2012;209:1457-68.

57. Carra S, Foglia E, Cermenati S, Bresciani E, Giampietro C, Lora Lamia C, Dejana E, Beltrame M and Cotelli F. Ve-ptp modulates vascular integrity by promoting adherens junction maturation. *PLoS One*. 2012;7:e51245.

58. Toselli CM, Wilkinson BM, Paterson J and Kieffer TJ. Vegfa/vegfr2 signaling is necessary for zebrafish islet vessel development, but is dispensable for beta-cell and alpha-cell formation. *Sci Rep*. 2019;9:3594.

59. Koenig AL, Baltrunaite K, Bower NI, Rossi A, Stainier DY, Hogan BM and Sumanas S. Vegfa signaling promotes zebrafish intestinal vasculature development through endothelial cell migration from the posterior cardinal vein. *Dev Biol*. 2016;411:115-27.

60. Wu BJ, Chiu CC, Chen CL, Wang WD, Wang JH, Wen ZH, Liu W, Chang HW and Wu CY. Nuclear receptor subfamily 2 group F member 1a (nr2f1a) is required for vascular development in zebrafish. *PLoS One*. 2014;9:e105939.

61. Mendelson K, Zygmunt T, Torres-Vazquez J, Evans T and Hla T. Sphingosine 1-phosphate receptor signaling regulates proper embryonic vascular patterning. *J Biol Chem*. 2013;288:2143-56.

62. Schindler YL, Garske KM, Wang J, Firulli BA, Firulli AB, Poss KD and Yelon D. Hand2 elevates cardiomyocyte production during zebrafish heart development and regeneration. *Development*. 2014;141:3112-22.
63. Nguyen AT, Xiao B, Neppl RL, Kallin EM, Li J, Chen T, Wang DZ, Xiao X and Zhang Y. DOT1L regulates dystrophin expression and is critical for cardiac function. *Genes Dev*. 2011;25:263-74.
64. Medrano JL and Naya FJ. The transcription factor MEF2A fine-tunes gene expression in the atrial and ventricular chambers of the adult heart. *J Biol Chem*. 2017;292:20975-20988.
65. Lazic S and Scott IC. Mef2cb regulates late myocardial cell addition from a second heart field-like population of progenitors in zebrafish. *Dev Biol*. 2011;354:123-33.
66. Liu J, Bressan M, Hassel D, Huisken J, Staudt D, Kikuchi K, Poss KD, Mikawa T and Stainier DY. A dual role for ErbB2 signaling in cardiac trabeculation. *Development*. 2010;137:3867-75.
67. Gerhart SV, Jefferis R and Iovine MK. Cx40.8, a Cx43-like protein, forms gap junction channels inefficiently and may require Cx43 for its association at the plasma membrane. *FEBS Lett*. 2009;583:3419-24.
68. Gemel J, Levy AE, Simon AR, Bennett KB, Ai X, Akhter S and Beyer EC. Connexin40 abnormalities and atrial fibrillation in the human heart. *J Mol Cell Cardiol*. 2014;76:159-68.
69. Gibb N, Lazic S, Yuan X, Deshwar AR, Leslie M, Wilson MD and Scott IC. Hey2 regulates the size of the cardiac progenitor pool during vertebrate heart development. *Development*. 2018;145.
70. Vermot J, Forouhar AS, Liebling M, Wu D, Plummer D, Gharib M and Fraser SE. Reversing blood flows act through klf2a to ensure normal valvulogenesis in the developing heart. *PLoS Biol*. 2009;7:e1000246.
71. Braun LJ, Zinnhardt M, Vockel M, Drexler HC, Peters K and Vestweber D. VE-PTP inhibition stabilizes endothelial junctions by activating FGD5. *EMBO Rep*. 2019.
72. Juettner VV, Kruse K, Dan A, Vu VH, Khan Y, Le J, Leckband D, Komarova Y and Malik AB. VE-PTP stabilizes VE-cadherin junctions and the endothelial barrier via a phosphatase-independent mechanism. *J Cell Biol*. 2019;218:1725-1742.
73. Dejana E, Tournier-Lasserve E and Weinstein BM. The control of vascular integrity by endothelial cell junctions: molecular basis and pathological implications. *Dev Cell*. 2009;16:209-21.
74. Jia W, Yao Z, Zhao J, Guan Q and Gao L. New perspectives of physiological and pathological functions of nucleolin (NCL). *Life Sci*. 2017;186:1-10.
75. Monte E, Mouillesseaux K, Chen H, Kimball T, Ren S, Wang Y, Chen JN, Vondriska TM and Franklin S. Systems proteomics of cardiac chromatin identifies nucleolin as a regulator of growth and cellular plasticity in cardiomyocytes. *Am J Physiol Heart Circ Physiol*. 2013;305:H1624-38.
76. Birmpas C, Briand JP, Courty J and Katsoris P. Nucleolin mediates the antiangiogenesis effect of the pseudopeptide N6L. *BMC Cell Biol*. 2012;13:32.
77. Watanabe T, Tsuge H, Imagawa T, Kise D, Hirano K, Beppu M, Takahashi A, Yamaguchi K, Fujiki H and Suganuma M. Nucleolin as cell surface receptor for tumor necrosis factor-alpha inducing protein: a carcinogenic factor of Helicobacter pylori. *J Cancer Res Clin Oncol*. 2010;136:911-21.
78. Ebos JM and Kerbel RS. Antiangiogenic therapy: impact on invasion, disease progression, and metastasis. *Nat Rev Clin Oncol*. 2011;8:210-21.
79. Roussel P and Hernandez-Verdun D. Identification of Ag-NOR proteins, markers of proliferation related to ribosomal gene activity. *Exp Cell Res*. 1994;214:465-72.
80. Hovanessian AG, Puvion-Dutilleul F, Nisole S, Svab J, Perret E, Deng JS and Krust B. The cell-surface-expressed nucleolin is associated with the actin cytoskeleton. *Exp Cell Res*. 2000;261:312-28.
81. Fonseca NA, Rodrigues AS, Rodrigues-Santos P, Alves V, Gregorio AC, Valerio-Fernandes A, Gomes-da-Silva LC, Rosa MS, Moura V, Ramalho-Santos J, Simoes S and Moreira JN. Nucleolin overexpression in breast cancer cell sub-populations with different stem-like phenotype enables targeted intracellular delivery of synergistic drug combination. *Biomaterials*. 2015;69:76-88.
82. Visvader JE and Lindeman GJ. Cancer stem cells: current status and evolving complexities. *Cell Stem Cell*. 2012;10:717-728.

83. Pattabiraman DR and Weinberg RA. Tackling the cancer stem cells - what challenges do they pose? *Nat Rev Drug Discov*. 2014;13:497-512.

84. Fonseca NA, Cruz AF, Moura V, Simoes S and Moreira JN. The cancer stem cell phenotype as a determinant factor of the heterotypic nature of breast tumors. *Crit Rev Oncol Hematol*. 2017;113:111-121.

85. Gregorio AC, Lacerda M, Figueiredo P, Simoes S, Dias S and Moreira JN. Meeting the needs of breast cancer: A nucleolin's perspective. *Crit Rev Oncol Hematol*. 2018;125:89-101.

86. Schwab MS and Dreyer C. Protein phosphorylation sites regulate the function of the bipartite NLS of nucleolin. *Eur J Cell Biol*. 1997;73:287-97.

87. Di Segni A, Farin K and Pinkas-Kramarski R. Identification of nucleolin as new ErbB receptors- interacting protein. *PLoS One*. 2008;3:e2310.

88. Wolfson E, Solomon S, Schmukler E, Goldshmit Y and Pinkas-Kramarski R. Nucleolin and ErbB2 inhibition reduces tumorigenicity of ErbB2-positive breast cancer. *Cell Death Dis*. 2018;9:47.

89. Das S, Cong R, Shandilya J, Senapati P, Moindrot B, Monier K, Delage H, Mongelard F, Kumar S, Kundu TK and Bouvet P. Characterization of nucleolin K88 acetylation defines a new pool of nucleolin colocalizing with pre-mRNA splicing factors. *FEBS Lett*. 2013;587:417-24.

90. Yelon D, Ticho B, Halpern ME, Ruvinsky I, Ho RK, Silver LM and Stainier DY. The bHLH transcription factor hand2 plays parallel roles in zebrafish heart and pectoral fin development. *Development*. 2000;127:2573-82.

91. Srivastava D, Cserjesi P and Olson EN. A subclass of bHLH proteins required for cardiac morphogenesis. *Science*. 1995;270:1995-9.

92. de Soysa TY, Ranade SS, Okawa S, Ravichandran S, Huang Y, Salunga HT, Schricker A, Del Sol A, Gifford CA and Srivastava D. Single-cell analysis of cardiogenesis reveals basis for organ-level developmental defects. *Nature*. 2019;572:120-124.

93. Anderson DJ, Kaplan DI, Bell KM, Koutsis K, Haynes JM, Mills RJ, Phelan DG, Qian EL, Leitoguinho AR, Arasaratnam D, Labonne T, Ng ES, Davis RP, Casini S, Passier R, Hudson JE, Porrello ER, Costa MW, Rafii A, Curl CL, Delbridge LM, Harvey RP, Oshlack A, Cheung MM, Mummery CL, Petrou S, Elefanty AG, Stanley EG and Elliott DA. NKX2-5 regulates human cardiomyogenesis via a HEY2 dependent transcriptional network. *Nat Commun*. 2018;9:1373.

94. Gerety SS and Anderson DJ. Cardiovascular ephrinB2 function is essential for embryonic angiogenesis. *Development*. 2002;129:1397-410.

95. Tobia C, Chiodelli P, Nicoli S, Dell'era P, Buraschi S, Mitola S, Foglia E, van Loenen PB, Alewijnse AE and Presta M. Sphingosine-1-phosphate receptor-1 controls venous endothelial barrier integrity in zebrafish. *Arterioscler Thromb Vasc Biol*. 2012;32:e104-16.

96. Duong TB, Ravisankar P, Song YC, Gafranek JT, Rydeen AB, Dohn TE, Barske LA, Crump JG and Waxman JS. Nr2f1a balances atrial chamber and atrioventricular canal size via BMP signaling-independent and -dependent mechanisms. *Dev Biol*. 2018;434:7-14.

97. Li W, Chen J, Deng M and Jing Q. The zebrafish Tie2 signaling controls tip cell behaviors and acts synergistically with Vegf pathway in developmental angiogenesis. *Acta Biochim Biophys Sin (Shanghai)*. 2014;46:641-6.

98. Sato TN, Tozawa Y, Deutsch U, Wolburg-Buchholz K, Fujiwara Y, Gendron-Maguire M, Gridley T, Wolburg H, Risau W and Qin Y. Distinct roles of the receptor tyrosine kinases Tie-1 and Tie-2 in blood vessel formation. *Nature*. 1995;376:70-4.

99. Eklund L, Kangas J and Saharinen P. Angiopoietin-Tie signalling in the cardiovascular and lymphatic systems. *Clin Sci (Lond)*. 2017;131:87-103.

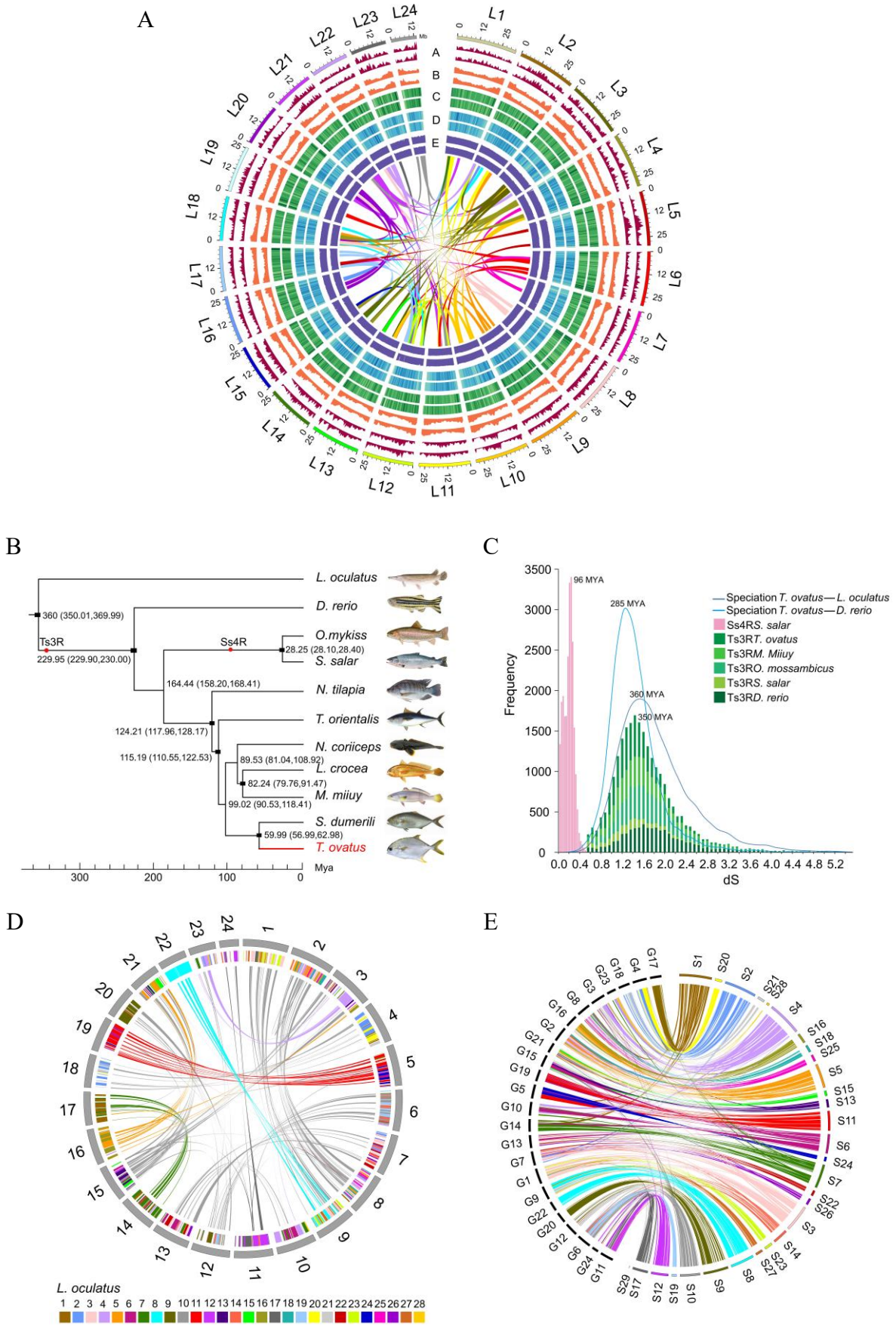

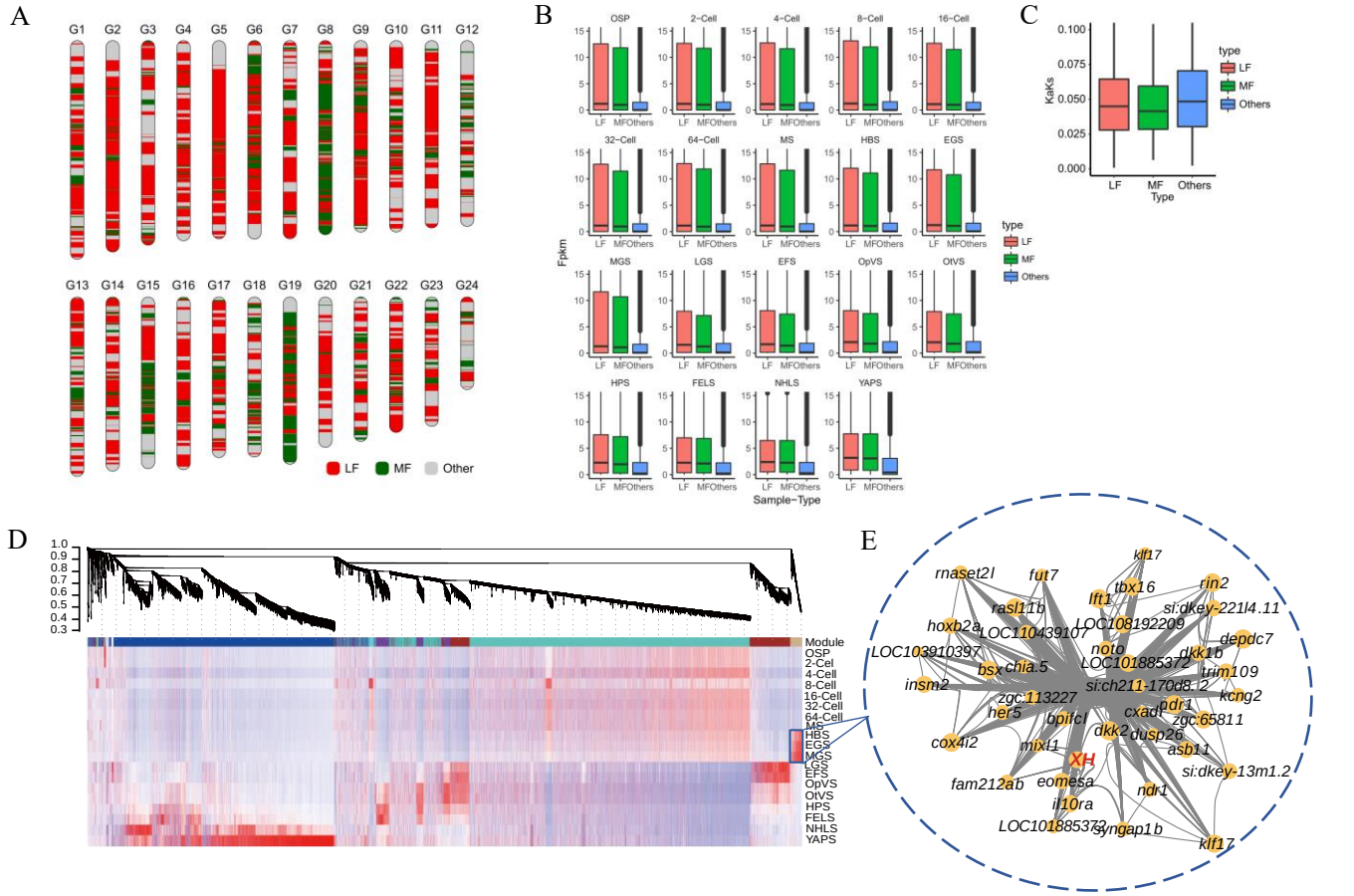

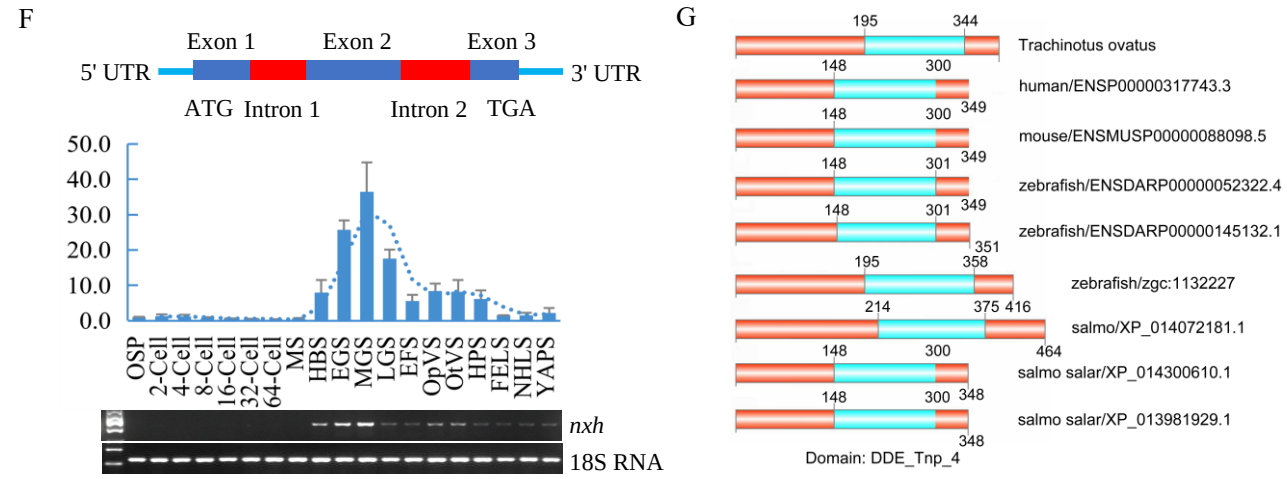

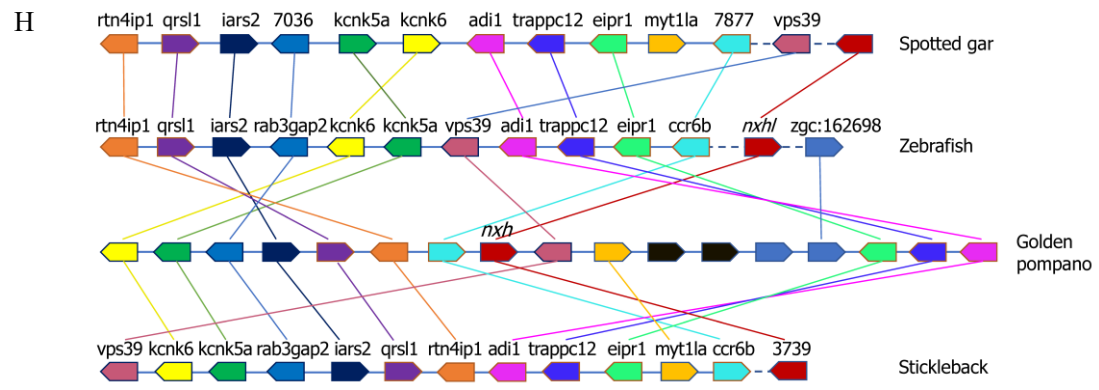

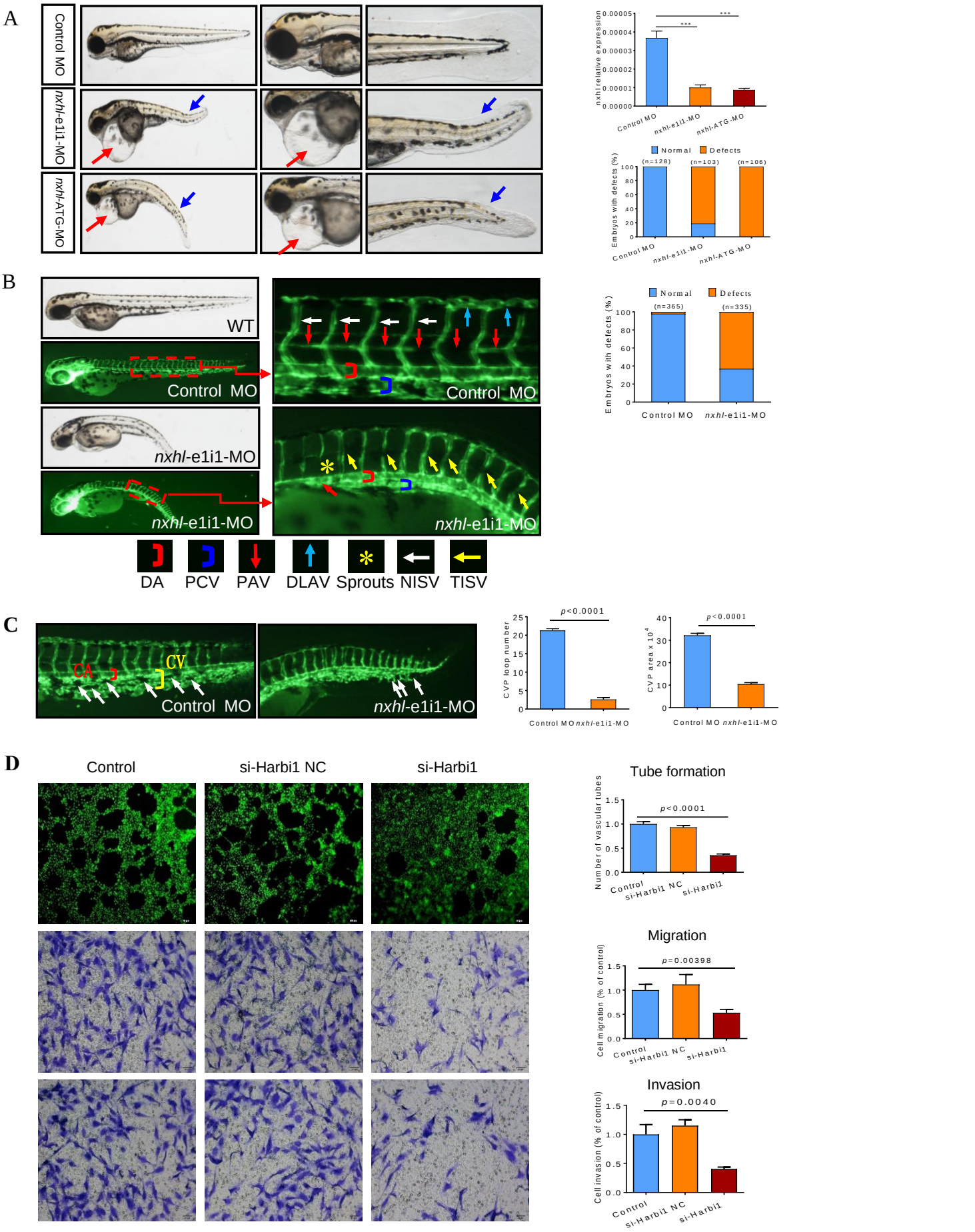

939

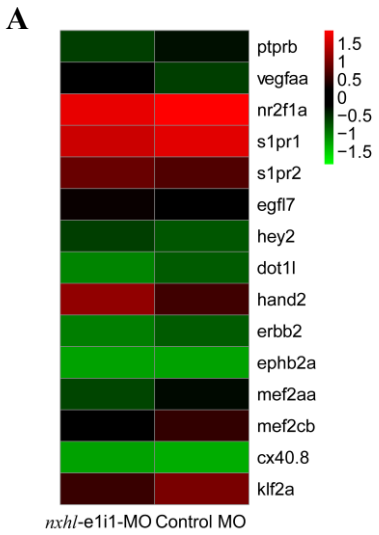

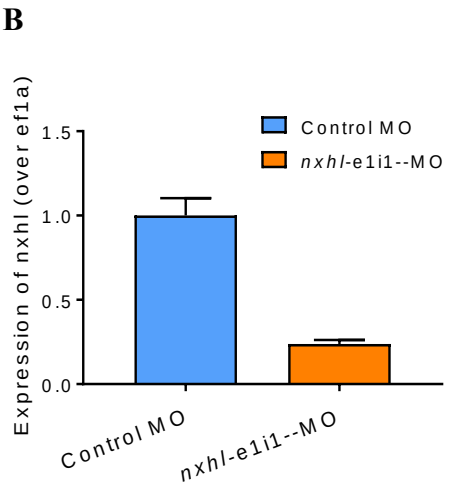

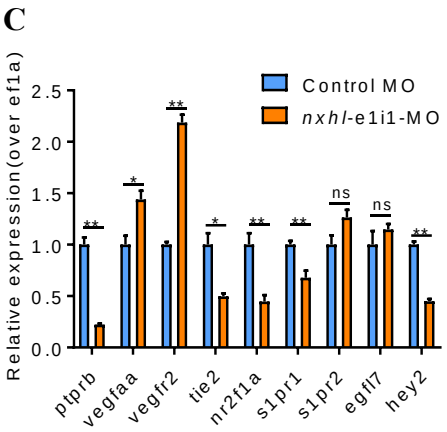

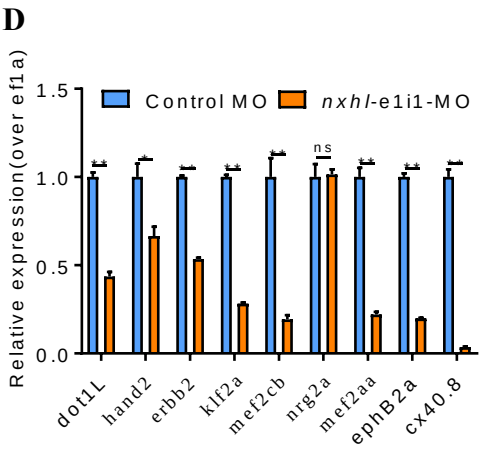

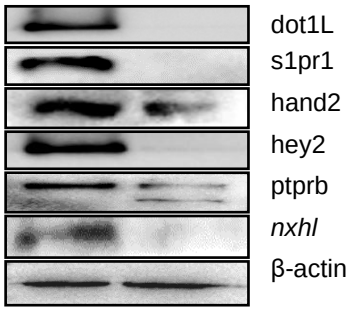

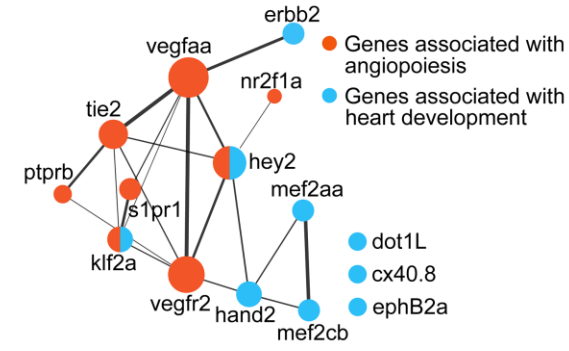

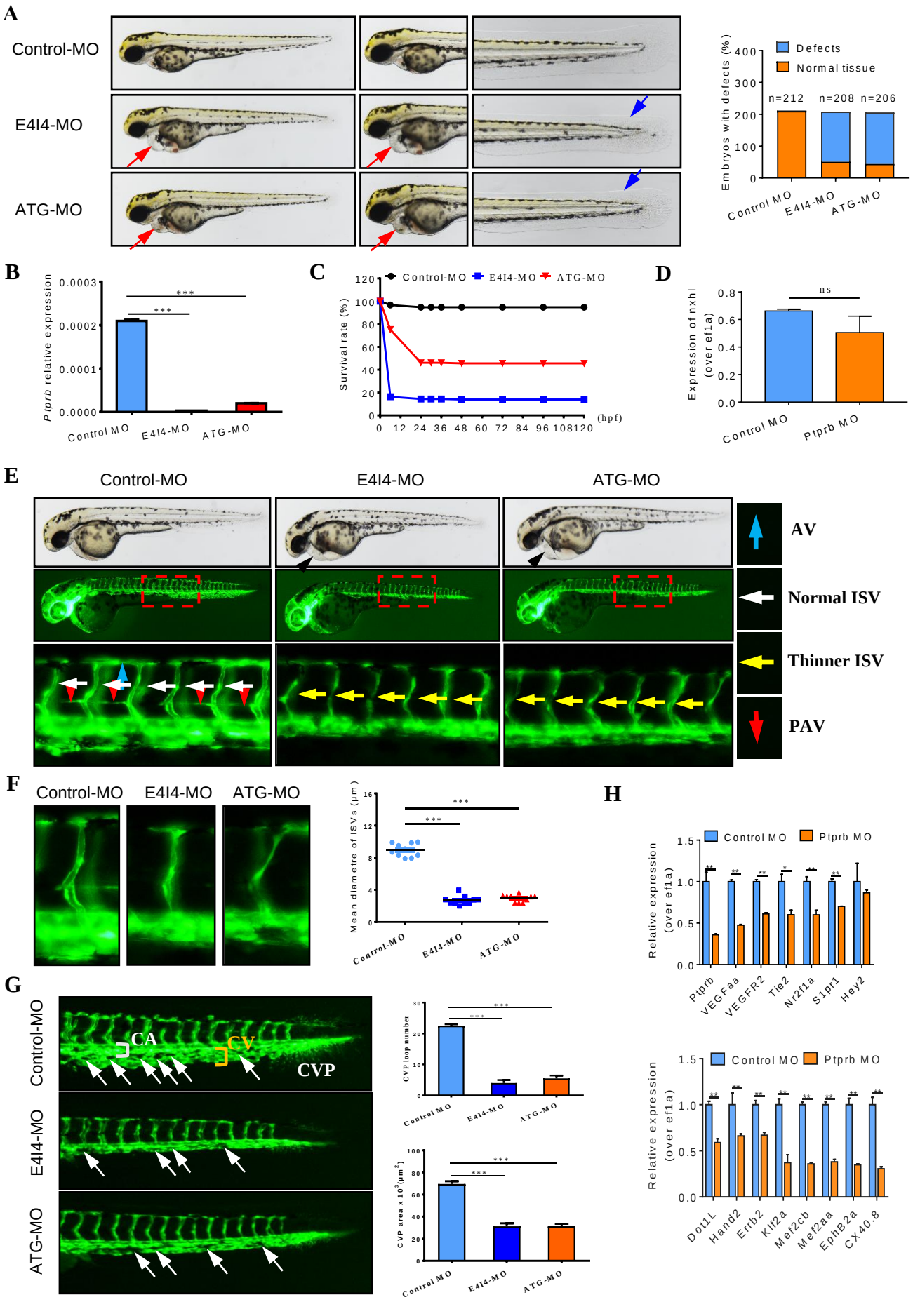

953

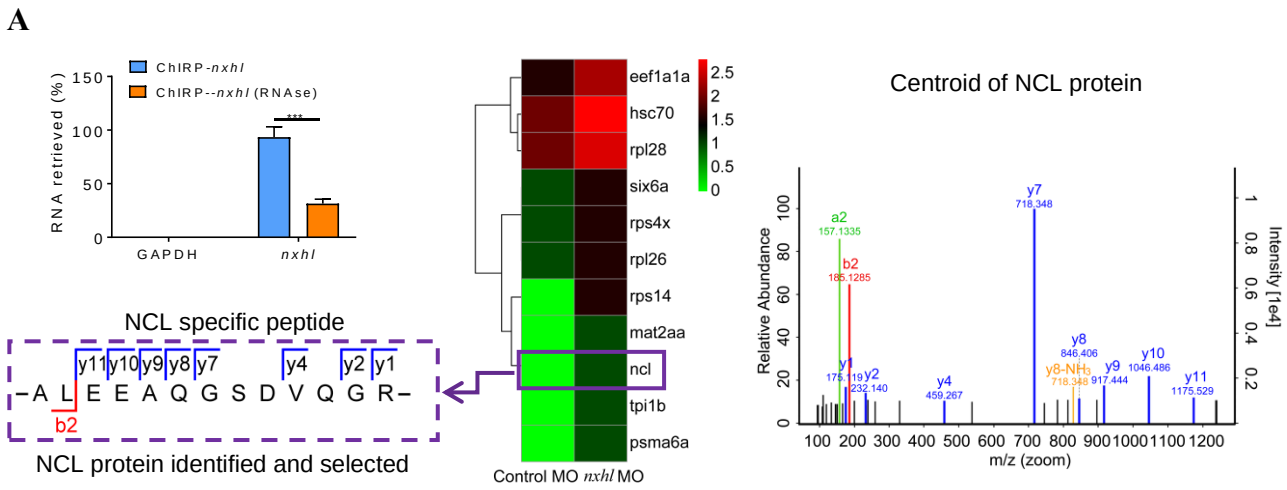

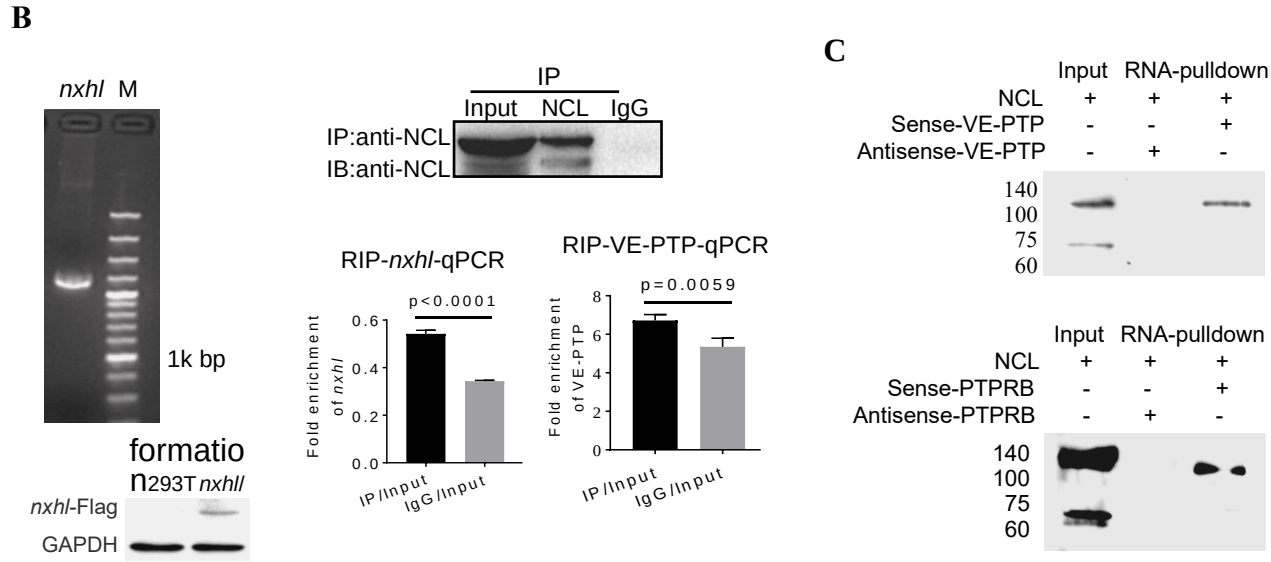

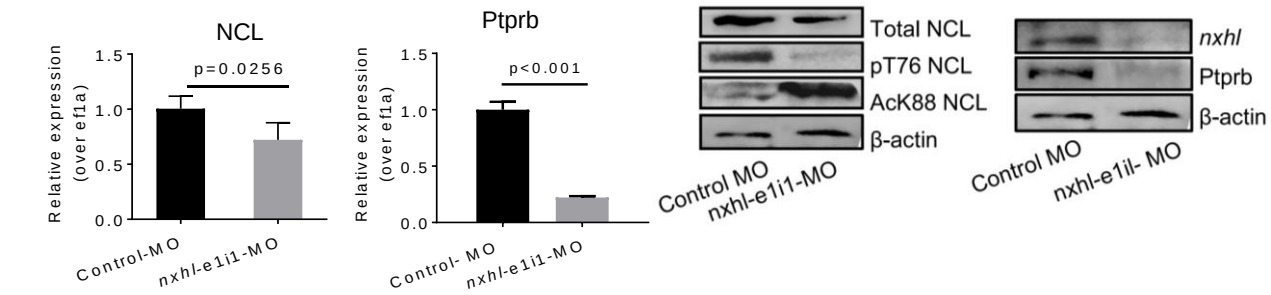

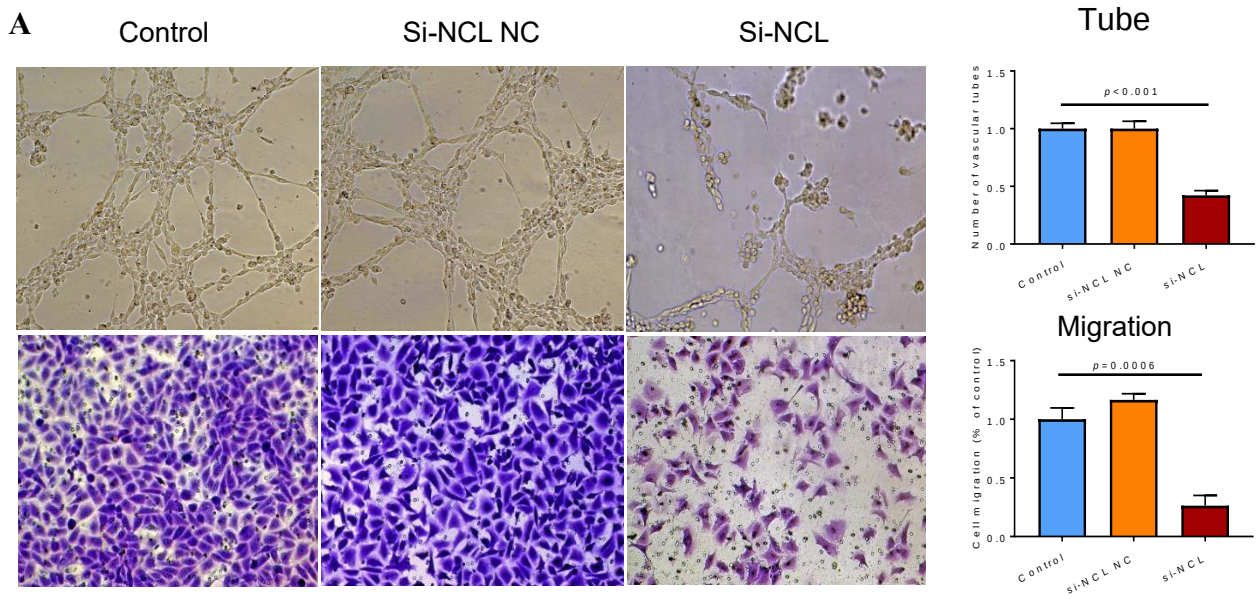

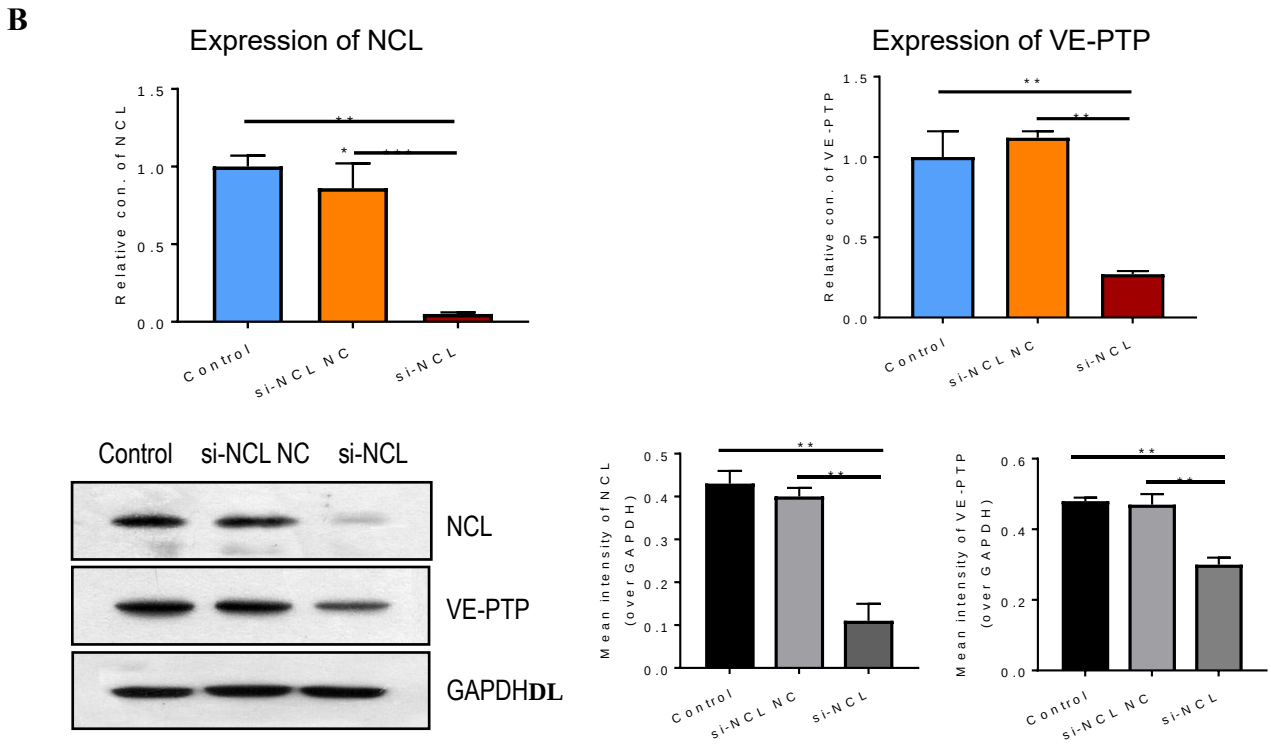

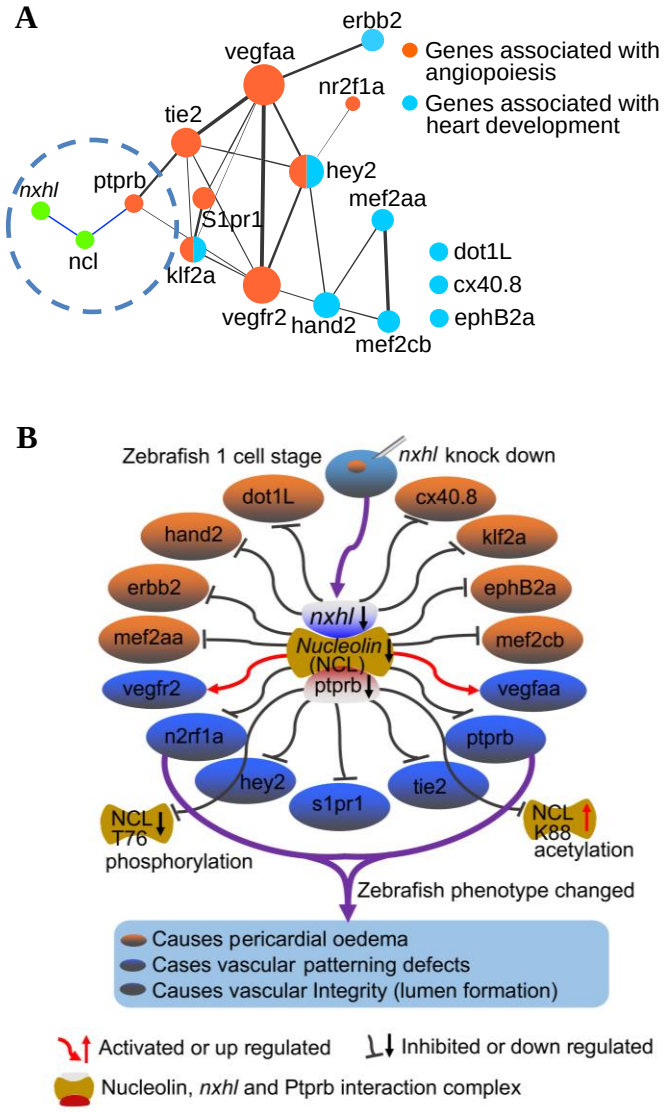

FIGURE LEGENDS

Figure 1. WGD of golden pompano notifies vertebrate karyotypes evolution. A, Overview of golden pompano (*Trachinotus ovatus)*. Numbers on the circumference are at the megabase scale. **a** Gene density of female *T. ovatus* (window size = 500 Kb). **b** TE content density of female *T. ovatus* (window size = 500 Kb). **c** Genome markers (optical) density of female *T. ovatus* (window size = 500 Kb). **d** Hi-C depth of female *T. ovatus* (window size = 500 Kb). **e** GC content of female *T. ovatus* (window size = 500 Kb). **f** Color bands in the middle of the Circos plot connect segmental duplication (minimum five gene pairs) from Teleost-specific

whole genome duplication (Ts3R) events. **B,** Phylogenetic relationship of Perciformes and relevant teleost lineages. The position of golden pompano is highlighted in red. Red circles represent the Teleost specific whole genome duplication (Ts3R), Salmonid-specific whole genome duplication (Ss4R), respectively. The divergence time was estimated using the nodes with calibration times derived from the Time Tree database, which were marked by a black rectangle. **C,** Inspection of whole genome duplication events based on synonymous mutation rate (Ks) distribution. The x axis shows the synonymous distance until a Ks cut-off of 5.2. **D,** Internal genome synteny of golden pompano. Double-conserved synteny between the golden pompano and spot gar genomes. Only genes anchored to chromosomes are represented. **E,** Macro-synteny comparison between spotted gar and golden pompano shows the overall one-to-two double-conserved synteny relationship between spotted gar to a post-Ts3R teleost genome.

Figure 2. *Nxhl* is a conserved homologue of *nxh* retained after WGD. A, Component of less fragment (LF) and major fragment (MF) subgenomes within golden pompano genome. **B**, Boxplot of expression level of LF, MF and Other gene sets. **C,** Selection bias associated with ancestral subgenomes fragmentation. The Ka/Ks values were calculated by orthologous pairs between golden pompano and spotted gar which is outgroup species without Ts3R genome duplication events. **D,** WGCNA analysis of embryonic development stages revealed gene-network modules enriched. **E,** Hub-gene network of the purple module. Size of the dots represents hubness. Color of the dots represents the increasing expression level from low to high. Bold text highlights the genes known for *nxh* (EVM0008813) gene. **F,** Validation of expression level for *nxh* by QPCR technology. 18s RNA was considered as internal marker. Gene structure of *nxh* was showed at upper region. **G,** Micro-synteny analysis of *nxh* locus among spotted gar, zebrafish, gold pompano and stickleback. Two inversions and one insertion occurred in *nxh* locus region of golden pompano genomes. **H,** Domains of *nxh* and other homologous protein. The domains were identified in SMART database (http://smart.embl.de/).

Figure 3. *Nxhl* affects angiogenic phenotypes *in vivo* and *in vitro*. A, Gross morphology at 3 dpf in wild-type AB strain. Knock down *nxhl* present pericardial oedema (red arrow) and caudal fin defects (blue arrow). The bar graph shows the validation of MO against *nxhl*, and the percentage of embryos with development defects after knockdown of *nxhl* with e1i1-MO and ATG-MO. **B,** knockdown of *nxhl* causes angiogenic defects in *Tg(fli1a:EGFP)*^{y1} zebrafish. Images represent bright field and fluorescent filed of *Tg(fli1a:EGFP)*^{y1} embryos at 52 hpf, with the angiogenic structures visualized by GFP fluorescence and labelled ISV and DLAV. The bar graph shows the percentage of embryos with angiogenic defects after knockdown of *nxhl* with *nxhl*-e1i1-MO. **C,** *nxhl* knockdown impairs formation of the CVP in zebrafish. Quantification of loop formation and area at CVP at 52 hpf. CA, caudal artery; CV, caudal vein. NISV, normal intersegmental vessel; TISV, thinner intersegmental vessel. **D,** Silence of Harbi1 inhibits angiogenic development *in vitro*. The tube formation, cell migration and invasion potential of HUVECs treated with si-Harbi1 was determined by using transwell chambers as described in the "Materials and methods" section. Scale bars, 50 μm. Representative images of cells stained in si-Harbi1 treated HUVEC cells. The data represent as mean±SEM from three independent experiments. *p<0.05 p<0.05, **p< 0.001 represents statistically significant.

Figure 4. *Nxhl* modulates *ptprb* expression and angiogenic networks. A, Heatmap of the 15 selected genes from zebrafishes after injection of 4ng *nxhl* ^{e1i1} MO at 3 dpf examined by RNA-seq. **B,** Expression of *nxhl* post injection of *nxhl* ^{e1i1} MO 3 dpf. **C,** Expression of genes associated with angiopoiesis post injection of *nxhl* ^{e1i1} MO 3 dpf using QPCR. **D,** Expression of genes associated with heart development post injection of *nxhl* ^{e1i1} MO 3 dpf using QPCR. **E,** Networks of the genes previously reported to be associated with angiopoiesis and heart development. Cytoscope V3.6.1 was used to build this network. **F,** Protein levels of the selected genes associated with angiopoiesis and heart development post injection of *nxhl* ^{e1i1} MO 3 dpf

by using Western blotting. β-actin antibody was used as internal control. The data above represent as mean±SEM from three independent experiments. *p<0.05 p<0.05, **p< 0.001 represents statistically significant.

Figure 5. Loss of *ptprb* phenocopies *nxhl* deficiency. A, Gross morphology at 3 dpf. Knock down *ptprb* present pericardial oedema (red arrow) and caudal fin defects (blue arrow). The bar graph shows the percentage of embryos with development defects after knockdown of *ptprb*. **B,** Endogenous *ptprb* in control and *ptprb* morphants were assessed by qPCR. **C,** A time-course plot of percent survival in control and *ptprb* morphants for 3 days. dpf, days post fertilization. **D,** Expression of *nxhl* post injection of *ptprb* MO 3 dpf. **E,** Morpholino knockdown of *ptprb* causes angiogenic defects. Representative bright field and fluorescent images of *Tg(fli1a:EGFP)*^{y1} embryos at 50 hpf with the vascular structures visualized by eGFP fluorescence and labelled ISV and DLAV. The boxed regions are shown at higher magnification in the bottom panels. **F,** Quantification of the mean diametre of ISVs shows significantly decrease in *ptprb*-MO injected embryos. Columns, mean; SEM (n =10; ANOVA;) DLAV, dorsal longitudinal anastomotic vessels; ISV, intersegmental vessel**. G,** *ptprb* knockdown impairs formation of the CVP in zebrafish. Bars show the quantification of loop formation and area at CVP. CA, caudal artery; CV, caudal vein. **H,** Expression of genes associated with angiopoiesis (above) and heart development (down) post injection of *ptprb* MO 50 hpf using QPCR. The data represent as mean±SEM from three independent experiments. *p<0.05 p<0.05, **p< 0.001 represents statistically significant.

Figure 6. *Nxhl* regulates VE-PTP (*ptprb*) through interactions with NCL. A, ChIRP-MS identification of *nxhl* RNA binding proteins. qPCR identification of *nxhl* RNA in the eluted RNAs. Graph shows more than 90% *nxhl* RNA was retrieved, and no GAPDH was detected. Heat map shows major proteins are

enriched and significantly (change fold >2 and p<0.05) retrieved by *nxhl* and control probes, analyzed by LC/MS-MS. NCL protein (purple boxed) was selected as candidate for follow-up study. The Centroid of NCL protein shows that NCL protein is pull down and identified by LC/MS-MS. The specific peptide identifies NCL protein. **B,** RIP-qPCR assay to detect the interaction between *nxhl*, VE-PTP mRNA and NCL protein. The mRNA expression of *nxhl* was determined by qPCR and Western blotting against Flag antibody was performed to identify the successful expression of pcDNA3.1- Flag-*nxhl* plasmid in 293T cells. Bars show the interaction between *nxhl* mRNA and NCL protein. The interaction between VE-PTP mRNA and NCL protein is shown too, and qPCR shows the detection for VE-PTP mRNA expression in the NCL-pulled down RNA. **C,** Pull down assay to detect the interaction between *nxhl*, VE-PTP mRNA and NCL protein. Gels show the interaction between VE-PTP mRNA and NCL protein. Western blotting was performed to detect NCL protein in the VE-PTP-biotin probe -pulled down proteins in 293T cells. The interaction between *ptprb* mRNA and NCL protein is shown too. **D,** Loss of *nxhl* affects the expression of NCL at both mRNA and protein levels. The mRNA expression of NCL and *ptpr* were determined by qPCR. The total NCL protein, phosphorylated NCL, acetylated NCL, total *nxhl* and *ptprb* protein were detected by Western blotting using specific NCL antibodies. The mRNA expression of *ptprb* was determined by qPCR. The data represent as mean±SEM from three independent experiments. **p*<0.05, *p*<0.05, ***p*< 0.001 represents statistically significant.

Figure 7. Silence of NCL inhibits angiogenesis and expression of VE-PTP *in vitro*. A, Silence of NCL inhibits angiogenesis of HUVECs *in vitro*. The tube formation and cell migration potential of HUVECs treated with si-NCL was determined by using transwell chambers as described in the "Materials and methods" section. Scale bars, 20 μm. Representative images of cells stained in si-NCL treated HUVEC cells. The data represent as mean±SEM from three independent experiments. **p*<0.05 *p*<0.05, ***p*< 0.001 represents

statistically significant. **B,** Silence of NCL inhibits the expression of VE-PTP at both mRNA and protein levels. The expression of NCL and VE-PTP was quantified by qPCR. Protein levels of NCL and VE-PTP were examined by using Western blotting post silence of NCL. GAPDH antibody was used as internal control. The gray intensities of the WB images were calculated and present as mean±SEM from three independent experiments. *p<0.05 p<0.05, **p< 0.001 represents statistically significant.

Figure 8. ***Nxhl*** **controls angiogenesis by targeting VE-PTP (*ptprb*)-related angiogenic genes. A,** Schematic model illustrating the mechanism of *nxhl* in zebrafish angiogenesis and heart development. The interactions between *nxhl* mRNA and NCL protein, NCL protein and *ptprb* mRNA are new-found interactions in this study. **B,** Possible mechanism of *nxhl* in zebrafish angiogenesis and heart development. Knockdown of *nxhl* may downregulate the *nxhl*-NCL-*ptprb* complex, subsequently regulate the proteins associated with angiogenesis and heart development, and finally result in heart pericardial oedema, vascular patterning and integrity defects.